nature cell biology

Microtubule-driven nuclear rotations promote meiotic chromosome dynamics

Nicolas Christophorou[1,2,5], Thomas Rubin[1,2,5], Isabelle Bonnet[3,4], Tristan Piolot[1,2], Marion Arnaud[1,2] and Jean-René Huynh[1,2,6]

At the onset of meiosis, each chromosome needs to find its homologue and pair to ensure proper segregation. In *Drosophila*, pairing occurs during the mitotic cycles preceding meiosis. Here we show that germ cell nuclei undergo marked movements during this developmental window. We demonstrate that microtubules and Dynein are driving nuclear rotations and are required for centromere pairing and clustering. We further found that Klaroid (SUN) and Klarsicht (KASH) co-localize with centromeres at the nuclear envelope and are required for proper chromosome motions and pairing. We identified Mud (NuMA in vertebrates) as co-localizing with centromeres, Klarsicht and Klaroid. Mud is also required to maintain the integrity of the nuclear envelope and for the correct assembly of the synaptonemal complex. Our findings reveal a mechanism for chromosome pairing in *Drosophila*, and indicate that microtubules, centrosomes and associated proteins play a crucial role in the dynamic organization of chromosomes inside the nucleus.

One central event at the onset of meiosis is the pairing of homologous chromosomes. This seemingly simple process requires complex mechanisms as homologous chromosomes need to find each other, align along their length and assess their homology before pairing[1,2]. Pairing is then reinforced by synapsis, that is, the assembly of the synaptonemal complex[3]. Synapsis is often followed by recombination events, which ensure exchange of parental genetic information and segregation of homologous chromosomes during the first meiotic anaphase. Although great progress has been made in recent years, uncovering the molecular mechanisms that promote homologous pairing has proved very challenging[4,5]. One reason is the exciting but bewildering diversity of mechanisms leading to pairing in different organisms[6]. For example, the starting sites of pairing and synapsis are the telomeres in mammals[7,8], whereas there are specific sequences defining pairing centres for each chromosome in *Caenorhabditis elegans*[9], and pairing starts at centromeres in *Drosophila*[4,5,10,11]. Meiotic chromosomes are further organized into telomere bouquets in yeast and mammals or clusters of centromeres in flies, whereby telomeres or centromeres aggregate on one side of the nucleus[12–14]. These different chromosome organizations imply different types of dynamic chromosome movement. Deciphering the successive steps of meiotic chromosome dynamics by live-imaging microscopy has been another challenge, especially in multicellular organisms. Only recently, cutting-edge time-lapse microscopy has allowed the description of rapid Dynein-dependent movements of pairing centres in *C. elegans*, and rotational movements of telomeres in mouse spermatocytes[15–19]. These mechanisms are different from the actin-dependent telomere movements in budding yeast and the microtubule-driven horsetail motions described in fission yeast[20,21]. Thus, although setting chromosomes in motion to facilitate pairing is a common theme, it is not possible to extrapolate the underlying mechanisms from one species to another[6].

In *Drosophila*, the pairing of meiotic chromosomes remains practically unexplored[22] partly because meiotic pairing was viewed as an extension of a pre-existing somatic pairing[22]. We and others have shown recently that this is not the case for autosomal chromosomes in germline stem cells and that homologous chromosomes are actively pairing in the mitotic region preceding entry into meiosis[23,24]. These events take place in a specialized structure called the germarium at the anterior tip of each ovary (Fig. 1a) that is itself organized into several functional regions[25]. The mitotic region, also called region 1, is at the anterior tip. There, germline stem cells (GSCs) divide asymmetrically to produce a new GSC and a cystoblast, which undergoes exactly four mitotic divisions to form a germline cyst made of 16 cells. These divisions are incomplete[26]. All 16 cells thus remain connected by ring canals and by a germline-specific organelle called the fusome made of endoplasmic reticulum-derived vesicles. The branched shape of the fusome is a useful marker to distinguish each stage, GSC,

[1]Department of Genetics and Developmental Biology, Institut Curie, F-75248 Paris, France. [2]CNRS UMR3215, Inserm, U934 F-75248 Paris, France. [3]Laboratoire Physico-Chimie, Institut Curie, F-75248 Paris, France. [4]CNRS UMR 168, UPMC, F-75248 Paris, France. [5]These authors contributed equally to this work. [6]Correspondence should be addressed to J.-R.H. (e-mail: jean-rene.huynh@curie.fr)

Received 16 May 2015; accepted 3 September 2015; published online 12 October 2015; DOI: 10.1038/ncb3249

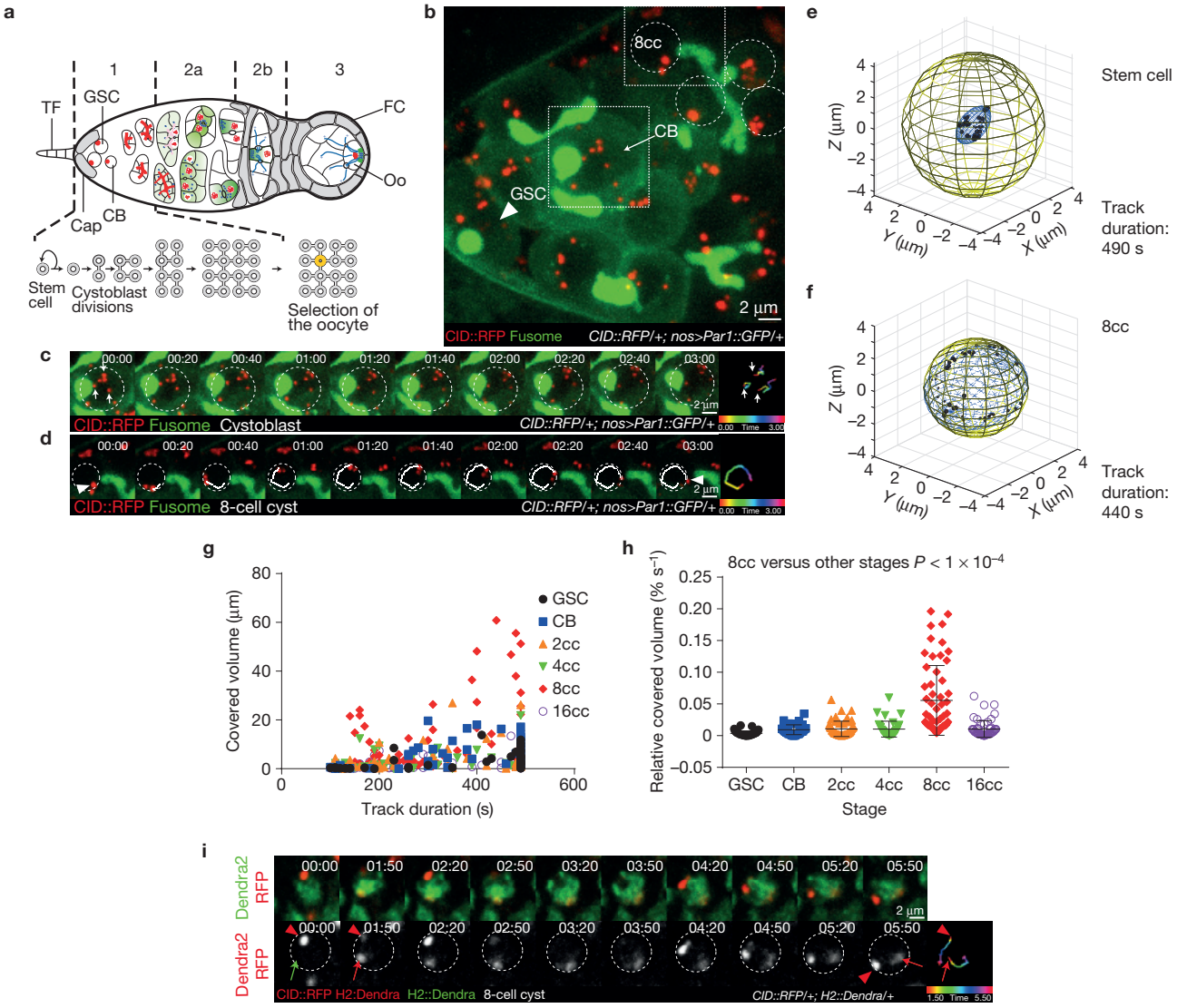

Figure 1 Centromeres and nuclei of 8-cell cysts exhibit a dynamic rotation behaviour. (**a**) GSCs at the anterior tip of the germarium (left) produce cystoblasts (CBs). The spectrosome (red circles) in GSCs and cystoblasts develops into a branched fusome. In early region 2a, the synaptonemal complex (red lines) forms along the chromosomes of the two cells with four ring canals (pro-oocytes, yellow) as they enter meiosis. By region 2b, the oocyte (Oo) is selected and is the only cell to remain in meiosis. TF, terminal filament; Cap, cap cells; FC, follicle cells. Blue dots are centrosomes migrating into the oocyte. Green shade shows the progressive restriction of some proteins or mRNAs into the oocyte. From ref. 23. (**b**) Projection of 11 *Z*-sections of a living germarium expressing CID::RFP (centromere, red) and Par1::GFP (fusome, green). GSC (arrowhead), cystoblast (arrow) and an 8-cell cyst (8cc), whose cells are linked by a fusome. Four nuclei of the 8-cell cyst are surrounded by dotted lines. (**c**,**d**) Selected projections from the outlined regions in **b** showing a single cystoblast nucleus (**c**) and a single 8-cell cyst nucleus (**d**) over a 3-min time course (nuclear surfaces are indicated by a dotted circle in each image). Time-coloured tracking images for three CID–RFP dots (arrows) in **c** and for one CID–RFP dot (arrowhead) in **d** are shown in the right panels. (**e**,**f**) Three-dimensional representations indicating the covered volume of one selected representative track for all time points; the ellipsoid is arbitrarily centred into a sphere representing the nuclear volume of a cystoblast (**e**) or an 8-cell cyst (**f**). (**g**) Raw covered volume plots for each track according to cyst stage. For each track, the total covered volume and the track duration are indicated along the *y* and *x* axes, respectively. (**h**) Distribution of the relative covered volume (raw covered volume/nuclear volume) per second for each track at different cyst stages (mean ± s.d., Mann–Whitney *U*-test comparing the wild-type 8-cell cyst with other stages $P < 1 \times 10^{-4}$, data were collected across 6 independent experiments). The number of analysed centromeric foci; stem cells: $n = 41$, cystoblasts: $n = 39$, 2-cell cysts: $n = 50$, 4-cell cysts: $n = 38$, 8-cell cysts: $n = 56$, 16-cell cysts: $n = 54$. (**i**) Selected projections showing a single 8-cell cyst nucleus over a 3-min time course. An ultraviolet pulse photoconverts Dendra2 from a green- to a red-emitting protein. Time-coloured tracking for one CID–RFP dot (red arrowhead) and one activated H2–Dendra dot (red arrow) is shown at the end of the time-lapse sequence. Time; minutes.

cystoblast, 2-, 4-, 8- and 16-cell cyst, in the mitotic zone. We showed that pairing between autosomal homologues mostly occurs during the 4-cell and 8-cell cysts[23,24]. In 16-cell cysts, paired centromeres of different chromosomes start to aggregate into one or two clusters at the nuclear envelope[10,11]. After the last mitosis, all 16 cells enter prophase I of meiosis in the meiotic zone of the germarium, also called region 2, and build some segments of synaptonemal complex. However, only one cell, the future oocyte, will remain in meiosis, while the 15 other

cells exit meiosis, endoreplicate their DNA and later become polyploid nurse cells.

In this study, we have improved further our technique of imaging live the germarium[27] to investigate whether there are chromosomal movements during meiotic pairing in *Drosophila* and to determine the molecular mechanisms driving homologous pairing in pre-meiotic germ cells.

RESULTS

Dynamic movements of centromeres and rolling nuclei in 8-cell cysts

While analysing the pairing and clustering of centromeres in pre-meiotic germ cells[23], we noticed that some centromeres showed coordinated and directional movements within specific nuclei. We followed each centromere with a CID–RFP fusion transgene and we labelled the fusome with a GFP-tagged marker to identify each stage of differentiation from GSCs to 16-cell cysts[28,29]. In GSCs, cystoblasts, 2-cell cysts and 4-cell cysts, most centromeres moved independently from each other and covered a small nuclear volume (Fig. 1b,c,e and Supplementary Video 1 and Supplementary Fig. 1A,B; and see Methods for quantification of centromere trajectories). In contrast, in 8-cell cysts, about 45% of centromeres showed coordinated circular movements (or revolutions) covering most of the nuclear space (Fig. 1b,d,f and Supplementary Video 1). Some centromeres could even undergo complete revolutions during one period of recording (Fig. 1g,h). These highly dynamic and directed movements were however transient as 16-cell cysts showed small covered volumes similar to 4-cell cysts (Fig. 1g,h).

We thus wondered whether the coordinated movements of centromeres were due to rotations of the entire nuclear envelope (NE) or whether centromeres were moving independently of the NE. When circular motions of centromeres were detected, we found similar and coordinated movements of nucleoporin foci on the NE (Supplementary Video 2). We concluded that the entire nuclear membrane was rotating. To test whether the entire nucleus, including all chromosomes, was also rotating, we made a Histone2A fused with a photoconvertible Dendra2 tag. This allowed us to label any sub-regions of chromatin in red with a brief pulse of a 405 nm laser (Fig. 1i). Simultaneous visualization of centromeres and labelled chromatin spots showed that both were moving in the same direction with the same speed (Fig. 1i and Supplementary Video 3). Thus, each nucleus rotates as a unit during a specific developmental window.

Microtubules are required for centromere dynamics

On the basis of studies done in *C. elegans*, *Schizosaccharomyces pombe*, maize and mouse, we reasoned that the microtubule cytoskeleton was a good candidate to drive these nuclear rotations[15,17,18,30,31]. We first examined in more detail the organization of microtubules in region 1 germline cysts. Using a GFP knock-in at an endogenous microtubule-associated protein (Jupiter) for live imaging, we found that the microtubule cytoskeleton was mainly organized around the fusome as previously published (Fig. 2a and Supplementary Video 4)[32,33]. We also observed microtubules around the nuclear envelope and emanating from centrosomes (Fig. 2a). Live imaging also allowed us to observe whip-like movement of microtubules in the cytoplasm (Supplementary Video 4). To decipher which structures were nucleating microtubules, we set up experimental conditions of live imaging where we could both inactivate and activate the microtubule cytoskeleton. We fed young female flies with the microtubule-polymerization inhibitor colcemid for 4 h and dissected the ovaries immediately. Germ cell microtubules were mostly depolymerized in such conditions and mitoses were arrested (Supplementary Video 5). Knowing that colcemid can be inactivated by ultraviolet light[34], we found that a 5 s ultraviolet pulse was sufficient to induce immediate re-growth of microtubules and rescue of mitoses (Supplementary Video 5). Microtubules were found to be growing from the fusome, centrosomes and nuclear envelopes (Fig. 2b and Supplementary Video 6). Thus, all three structures can nucleate microtubules, although most microtubules localize along the fusome.

During these recordings, we also noticed that centrosomes exhibited circular movements mainly in 8-cell cysts reminiscent of nuclear rotations (Supplementary Video 7). At this stage, 35% of centrosomes showed these rotations, while 65% remained static (Fig. 2c), which was similar to centromere behaviour (45% dynamic and 55% static). We thus imaged both centromeres and centrosomes simultaneously (using Cid::RFP and asterless::YFP, respectively) and found that most dynamic centrosomes underwent revolutions in the same direction and with the same speed as centromeres of the same cell (87% of co-rotation; Fig. 2d,g). However, during these co-rotations, centromeres and centrosomes were not co-localized at the nuclear envelope (28% of dynamic co-localization; Fig. 2e). In contrast, in static nuclei, centromeres and centrosomes often co-localized (Fig. 2f); and were associated with the fusome, as we and others had published for centrosomes[32,33,35].

In the presence of colcemid both centromere movements and relative covered volumes were markedly reduced in 8-cell cysts (Fig. 2h,j,k and Supplementary Video 8). Furthermore, on ultraviolet irradiation, the coordinated and directional movements of centromeres were immediately restored (Fig. 2i,j′ and Supplementary Video 9). We made similar observations for centrosome movements (Fig. 2b and Supplementary Video 10). In contrast, no change in centromere dynamics was observed in GSCs before and after the ultraviolet pulse (Supplementary Fig. 2 and Supplementary Video 11). Thus, centromere movements in 8-cell cysts depend on microtubules.

Centrosomes and Dynein are required for centromere dynamics

We used the fact that *Drosophila* germ cells can develop without centrosomes[36] and removed centrosomes genetically by knocking down *sas-4* and *asterless* (*asl*), which are required for centriole duplication[37,38]. We found that in both *sas-4*_shRNA and *asl*_shRNA mutant 8-cell cysts (small hairpin RNA, TRiP collection[39]), centromeres were still revolving but at a lower speed compared with control flies expressing a shRNA against *white* (Fig. 3a–c,e–g and Supplementary Videos 12–14). As a result, the relative covered volume per second was significantly reduced in knockdown conditions (Fig. 3i). We conclude that centrosomes are required for efficient nuclear rotations, but are not the main driving force.

To test for a potential function of the minus-end-directed motor Dynein in driving nuclear rotations, we used two independent transgenic lines expressing shRNA targeting *dynein* in germ cells (Fig. 3d,h and Supplementary Video 15). The movement of centromeres exhibited a marked reduction in the nuclear volume

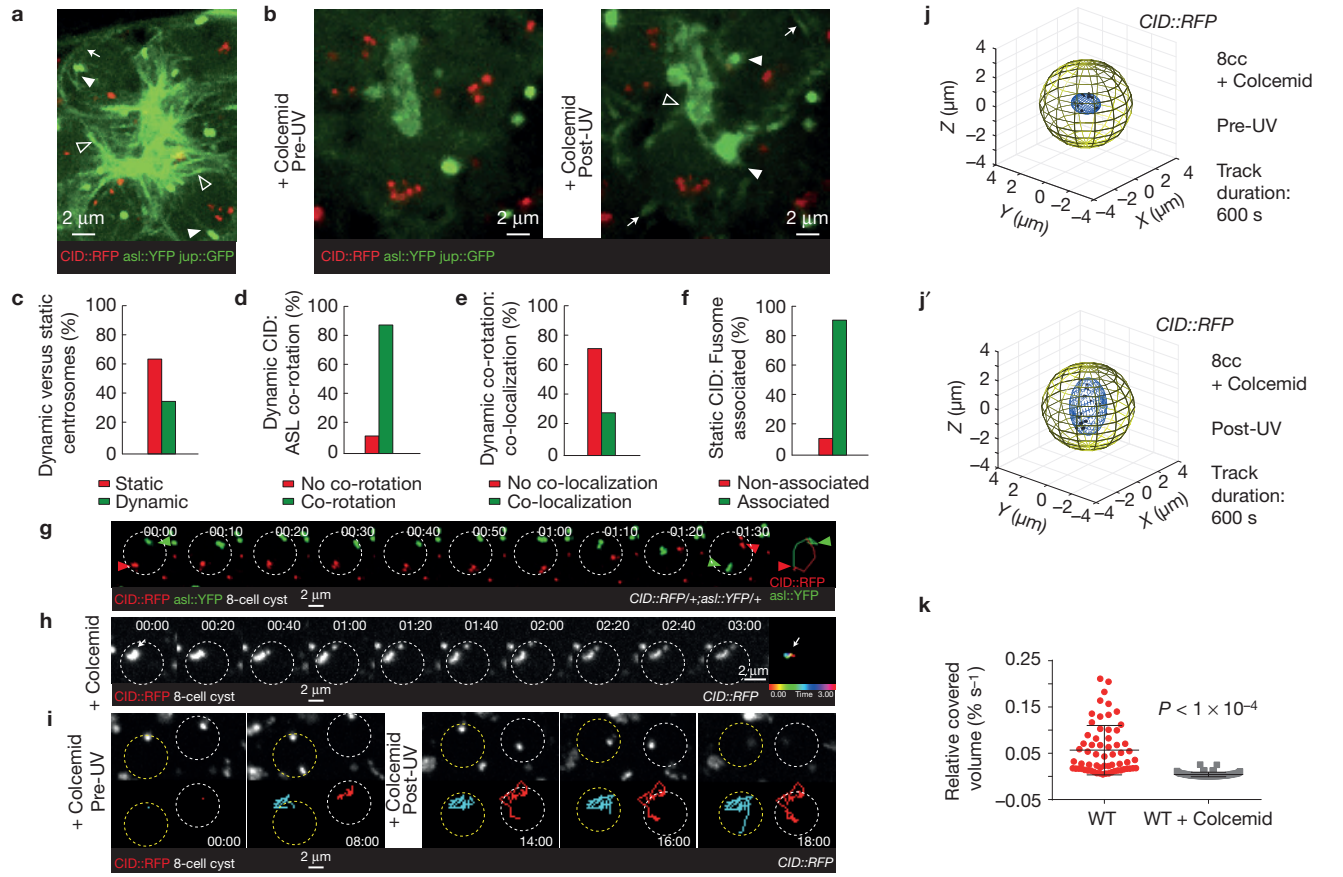

Figure 2 Microtubules drive centromere movements. (**a**) *Z*-projection of CID::RFP (centromeres, red), asl::YFP (centrosomes, yellow) and Jupiter::GFP (microtubules, green). Microtubules emanate from the fusome (empty arrowhead), nuclear membrane (arrow) and centrosomes (filled arrowhead). (**b**) *Z*-projection of CID::RFP (centromeres, red), asl::YFP (centrosomes, yellow) and Jupiter::GFP (microtubules, green). Immediately after a 5 s ultraviolet pulse, microtubules re-grow from the fusome (empty arrowheads), centrosomes (filled arrowheads) and nuclear membrane (arrow). (**c**) 35% of centrosomes exhibited rotations, while 65% remained static. (**d**) 87% of centrosomes were rotating in the same direction and with the same speed as centromeres of the same cell. (**e**) During these co-rotations, centromeres and centrosomes co-localized at the nuclear envelop in only 28% of cases examined. (**f**) In static nuclei, centromeres and centrosomes co-localized and were associated with the fusome in 91% of cases examined. (**g**) Selected projections showing a single 8-cell cyst nucleus over a 1.5-min time course. Centrosomes (asl::YFP, green) and centromeres (CID::RFP, red). Centrosomes rotate in the same direction and with the same speed as centromeres. Coloured tracking for one CID–RFP dot (red arrowhead) and one centrosome dot (green arrowhead) is shown on right panel. (**h**) Selected *Z*-projection of a single 8-cell cyst nucleus expressing *CID::RFP* over a 3-min time course (nuclear surface is indicated by a dotted circle in each image). Right panel: time-coloured tracking (arrow). (**i**) Inactivation of colcemid leads to re-establishment of CID foci dynamics in 8-cell cysts. Selected *Z*-projections of a single 8-cell cyst nucleus are shown. In the first two projections colcemid is active, microtubules are depolymerized and centromeric foci movement is very limited. In the last three projections colcemid was inactivated and centromeric movement is gradually restored. For each time point, the cumulative tracking is represented in the bottom half of the picture. The yellow and white dotted circles indicate the nuclear surface of two nuclei in each image. (**j**,**j′**) Three-dimensional representations indicating the covered volume of one representative track (yellow nucleus); the ellipsoid is arbitrarily centred into a sphere representing the nuclear volume of an 8-cell cyst (8cc) nucleus before the ultraviolet pulse (**j**) and the same 8-cell cyst after the ultraviolet pulse (**j′**). (**k**) The relative covered volume (raw covered volume/nuclear volume) per second in 8-cell cyst nuclei treated with colcemid is strongly reduced compared with wild-type 8-cell cysts (mean ± s.d., Mann–Whitney *U*-test, $P < 1 \times 10^{-4}$; WT: $n = 63$ centromeric foci; data collected across 6 independent experiments, WT + colcemid: $n = 75$ centromeric foci; data collected across 7 independent experiments).

covered and no rotational movements were seen in 8-cell cysts expressing *nanos:Gal4;UAS:Dhc*_shRNA (Fig. 3d,h,i and Supplementary Video 14). We confirmed these defects by using a viable but sterile combination of dynein alleles, $Dhc64c^{3\text{-}2}/Dhc64c^{6\text{-}12}$, in which we never observed any rotation (Fig. 3i and Supplementary Video 16). We further noticed that whip-like movements of microtubules were strongly reduced in this mutant condition (Supplementary Video 17 compared with Supplementary Video 4 for the wild-type condition). We conclude that microtubules and Dynein play a crucial role in generating nuclear rotations in pre-meiotic germ cells.

Microtubules, centrosomes and Dynein are required for centromere pairing, clustering and homologous chromosome synapsis

We previously showed that centromere pairing and clustering occurred most prominently at the 8-cell cyst stage, which is when we detected most nuclear rotations[23]. We wanted to test whether there was a functional connection between these two events. We thus assayed the effect of reducing microtubules, centrosomes and Dynein activity on centromere pairing and clustering, and on the formation of the synaptonemal complex. *Drosophila* diploid cells have

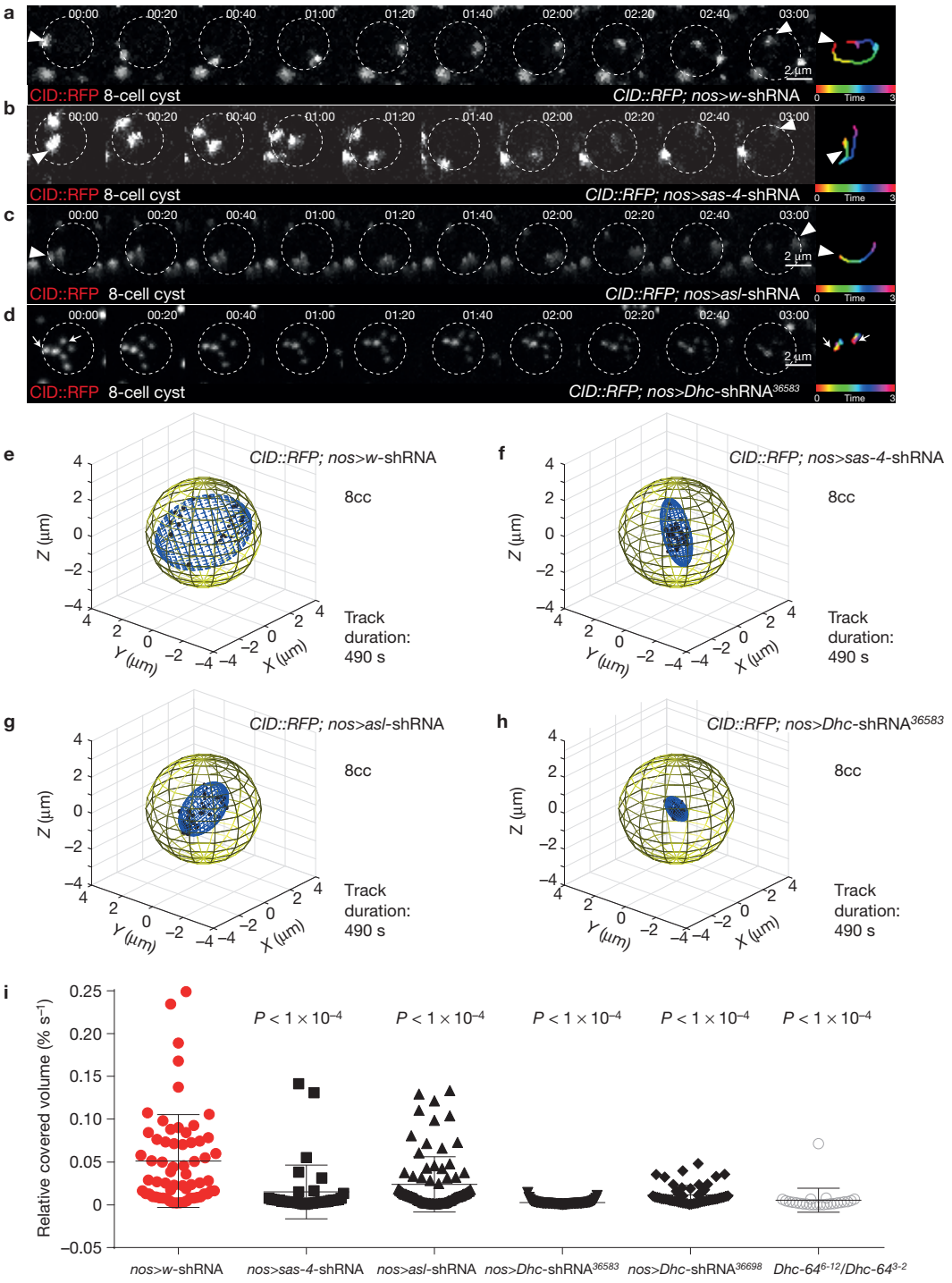

Figure 3 *sas-4*, *asl* and *Dynein* loss of function affects centromere dynamics. (**a**–**d**) Loss of function of Sas-4 and Asl (centrosomes) and Dynein by RNAi leads to inhibition of CID foci dynamics in living 8-cell cysts. Selected projections of *Z*-sections obtained by time-lapse microscopy (spinning disc) of a *CID–RFP; nos>w*-shRNA (**a**), *CID–RFP/sas-4*-shRNA;*nos-Gal4/+* (**b**), *CID–RFP/asl*-shRNA; *nos-Gal4/+* (**c**) and *CID–RFP/dhc64c*-shRNA^{36583}; *nos-Gal4/+* (**d**) germarium exhibiting a single 8-cell cyst nucleus over a 3-min time course (nuclear surface is indicated by a dotted circle in each image) are shown. Time-coloured tracking images of one or two CID–RFP dots (arrowhead or arrows) are shown at the end of the time-lapse sequence. (**e**–**h**) Three-dimensional representations indicating the covered volume of one selected representative track for all time points of a *CID–RFP; nos>w*-shRNA nucleus (**e**), a *CID–RFP/sas-4*-shRNA;*nos-Gal4/+* (**f**), a *CID–RFP/asl; nos-Gal4/+* (**g**) and a *CID–RFP/Dhc64c*-shRNA^{36583}*IR; nos-Gal4/+* nucleus (**h**). The ellipsoid is arbitrarily centred into a sphere representing the nuclear volume (gold sphere). 8cc, 8-cell cyst. (**i**) Distribution of the relative covered volume (raw covered volume/nuclear volume) per second of centromere foci in wild-type, shRNAs for *sas-4*, *asl* and *dhc64c*, and *Dhc64C*$^{3-2}$*/Dhc64C*$^{6-12}$ mutant germaria (mean ± s.d.; Mann–Whitney *U*-test $P < 1 \times 10^{-4}$; *nos>w*-shRNA $n = 44$ centromeric foci; data collected across 6 experiments, *nos>sas-4*-shRNA $n = 37$ centromeric foci/5 experiments, *nos>asl*-shRNA $n = 80$ centromeric foci/5 experiments *nos>Dhc*-shRNA^{36583} $n = 55$ centromeric foci/5 experiments, *nos>Dhc*-shRNA^{36698} $n = 55$ centromeric foci/5 experiments, *Dhc-64*$^{6-12}$*/Dhc-64*$^{3-2}$ $n = 24$ centromeric foci/3 experiments).

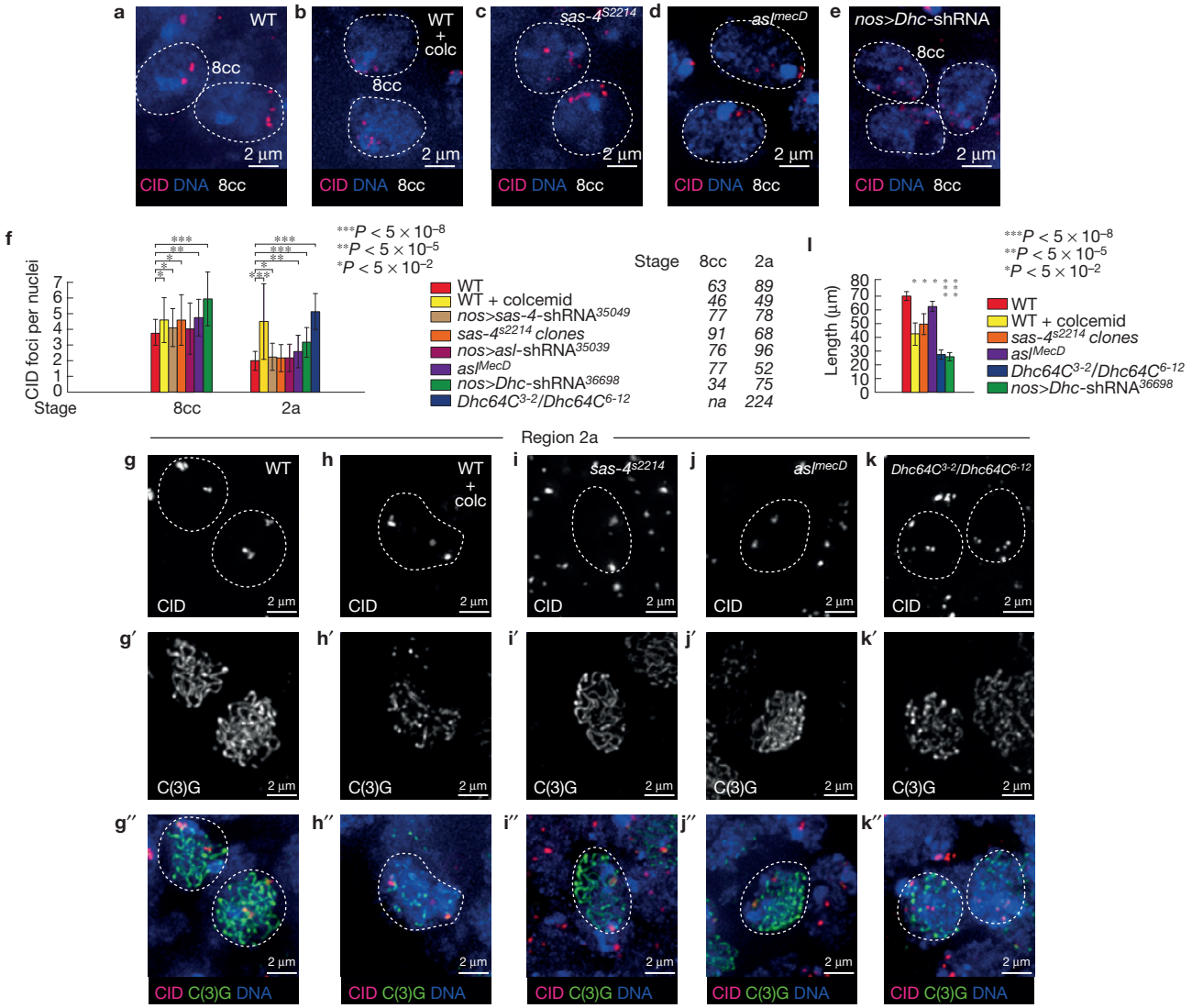

Figure 4 Microtubules, centrosomes and Dynein are required for centromere pairing in 8-cell cysts (8cc) and assembly of the synaptonemal complex. (**a**–**e**) Projection of *Z*-sections obtained by deconvolution microscopy of a wild-type (**a**), colcemid-treated (**b**), *sas-4*^{S2214} (**c**), *asl*^{mecD} (**d**) and *nos-Gal4>Dhc64C*-shRNA^{36698} (**e**) fixed germarium stained for centromeres (CID, red), and DNA. 8-cell cyst nuclei are indicated by a dotted circle in each image. (**f**) Developmental changes in the number of CID foci in 8-cell cyst nuclei and in pachytene nuclei in region 2a in wild-type, colcemid-treated and in different mutant and RNAi conditions. The number of analysed cells (*n*) is indicated for each stage on the right panel (data were collected across 3 independent experiments for each genotype; mean ± s.d.; two-tailed Student's *t*-test, $^{*}P < 5 \times 10^{-2}$, $^{**}P < 5 \times 10^{-5}$, $^{***}P < 5 \times 10^{8}$). (**g**–**k**″) Projection of *Z*-sections obtained by deconvolution microscopy of a wild-type (**g**–**g**″), colcemid-treated (**h**–**h**″), *sas-4*^{S2214} (**i**–**i**″), *asl*^{mecD} (**j**–**j**″) and *nos-Gal4>Dhc64C*-shRNA^{36698} (**k**–**k**″) fixed germaria stained for centromeres (CID, red) and the synaptonemal complex (C(3)G, green). (**l**) Length of the synaptonemal complex in colcemid-treated, dynein loss of function, and centrosome-mutant germaria, compared with the wild type (*y* axis is in µm; $n = 5$ independent nuclei for each genotype; mean ± s.d.; two-tailed Student's *t*-test, $P < 0.01$).

four pairs of homologues, and thus eight chromosomes. Therefore, when all homologues are paired, four dots of CID can be distinguished. More than four dots are seen when not all centromeres are paired, and when centromeres become clustered, one should see only one or two dots[10,11]. In wild-type 8-cell cyst nuclei, we counted an average number of CID foci of 3.8 ± 0.8 (Fig. 4a,f) indicating that most chromosomes were paired and started to cluster at their centromeres. Colcemid treatment caused a significant increase in CID foci with an average of 4.7 ± 1.5 (Fig. 4b,f). Similarly, in the absence of centrosomes, the number of CID foci was increased to 4.7 ± 1.6 in the *sas-4* mutant and 4.8 ± 1.2 in the *asl* mutant (Fig. 4c,d,f). In germaria expressing *nanos:Gal4;UAS:Dhc*_shRNA, CID foci increased to 6.0 ± 1.7 (Fig. 4e,f).

Analysis of centromere clustering and synaptonemal complex assembly in meiotic nuclei of region 2a showed that wild-type pachytene nuclei exhibited an average number of 2.0 ± 0.6 CID foci per nucleus (Fig. 4f,g). In the absence of centrosomes, we noticed a minor increase in the number of CID dots, 2.2 ± 0.9 and 2.6 ± 1 in *sas-4* and *asl* mutant flies respectively (Fig. 4f). The presence of colcemid exacerbated the phenotype (4.4 ± 2.4 dots) and when Dynein activity was disrupted either by RNA-mediated interference (RNAi; 3.2 ± 0.9 dots) or using viable but sterile combination of *dynein* alleles,

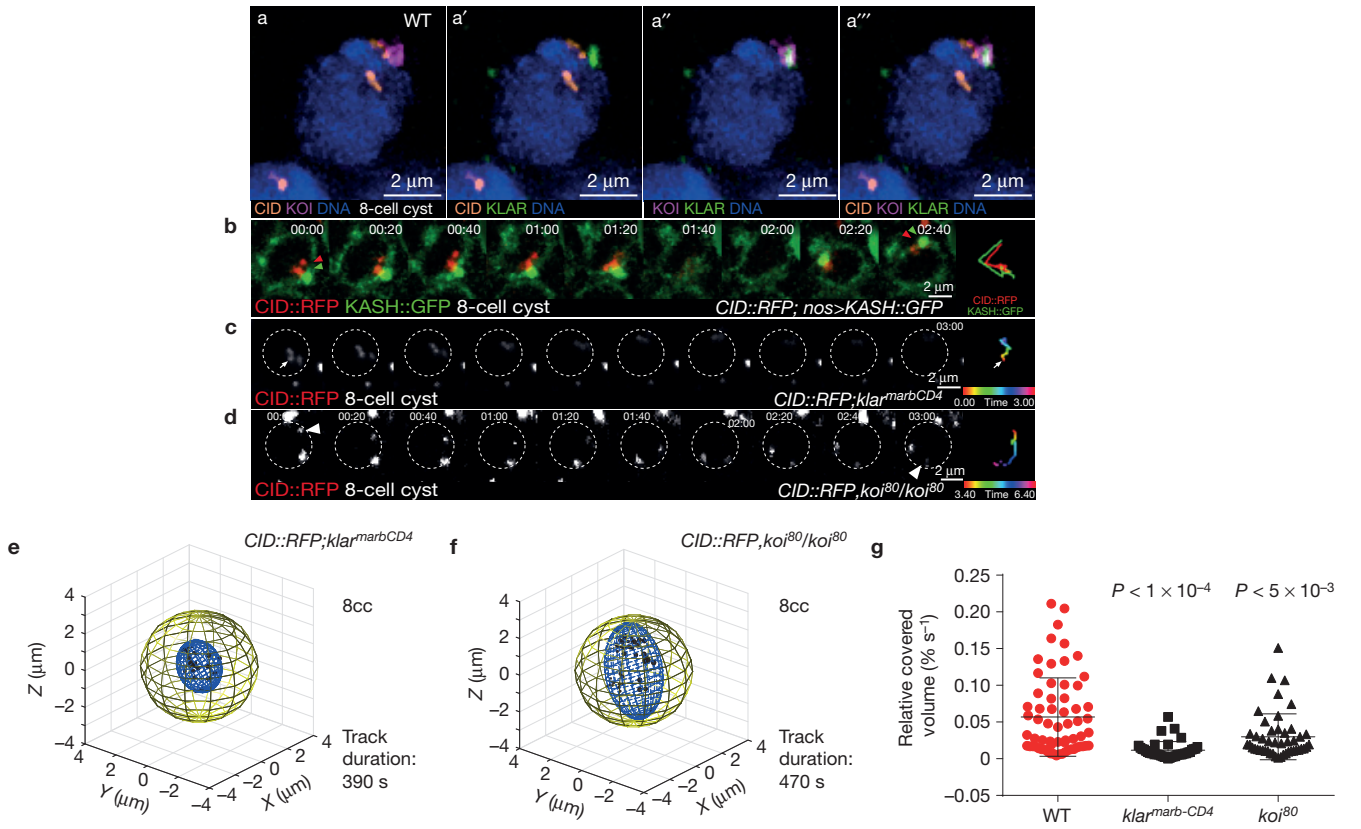

Figure 5 Klarsicht and Klaroid are present near centromeres in the mitotic region and are differentially required for chromosome movements. (**a**–**a‴**) Projection of *Z*-sections obtained by deconvolution microscopy of a wild-type 8-cell cyst stained for centromere (CID, orange), Klarsicht (Klar, green), Klaroid (Koi, magenta) and DNA (DAPI, blue). (**b**) Selected projections of 5 *Z*-sections obtained by time-lapse microscopy (confocal) of a living CID–RFP; nos>UAS-KASH-GFP germarium showing a single 8-cell cyst nucleus over a 3-min time course. Coloured tracking for one CID–RFP dot (arrowhead, red) and one KASH-GFP dot (arrowhead, green) is shown at the end of the time-lapse sequence. (**c**,**d**) Selected projections of *Z*-sections obtained by time-lapse microscopy (spinning disc) of a *CID::RFP/+;klar*^{mbCD4} (**c**) and *CID::RFP,koi*^{80}*/koi*^{80} (**d**) germarium exhibiting single 8-cell cyst nuclei over a 3-min time course (nuclear surface is indicated by a dotted circle in each image) are shown. Time-coloured tracking images of CID–RFP dots (arrowhead or arrow) are shown at the end of the time-lapse sequence. (**e**,**f**) Three-dimensional representations indicating the relative covered volume of one selected representative track for all time points of a *CID::RFP/+;klar*^{mbCD4} (**e**), and a *CID::RFP,koi*^{80}*/koi*^{80} (**f**) 8-cell cyst (8cc) selected nucleus. The ellipsoid is arbitrarily centred into a sphere representing the nuclear volume (gold sphere). (**g**) Distributions of the relative covered volume per second for centromeric foci in *CID–RFP*, *CID::RFP/+;klar*^{mbCD4}, and *CID::RFP,koi*^{80}*/koi*^{80} 8-cell cyst nuclei (mean ± s.d., Mann–Whitney *U*-test $P < 1 \times 10^{-3}$; WT: $n = 63$ centromeric foci; collected across 6 independent experiments, *klar*^{marcCD4}: $n = 40$ centromeric foci/3 independent experiments, *koi*^{80}: $n = 47$ centromeric foci/3 independent experiments).

Dhc64c$^{3\text{-}2}$*/Dhc64c*$^{6\text{-}12}$, (5.1 ± 1.2 dots of CID, Fig. 4f). However, even after long exposures to colcemid, centromeres managed to pair later during oogenesis, in region 2b (Supplementary Fig. 3).

In the presence of colcemid and in both *nanos>Dhc*_shRNA and *Dhc64c*$^{3\text{-}2}$*/Dhc64c*$^{6\text{-}12}$ flies, the synaptonemal complex of all meiotic nuclei looked fragmented with shorter filaments (Fig. 4h,k). The total length of synaptonemal complex fragments per cell was reduced by half under these conditions compared with the wild type (Fig. 4l). In *sas-4* and *asl* mutant ovaries, the phenotype was much less pronounced. The total synaptonemal complex length per cell was nonetheless slightly shorter than in wild-type conditions and the normalized intensity was reduced (Fig. 4l and Fig. 6j).

We conclude that centrosomes play a secondary role in promoting pre-meiotic pairing, centromere clustering and synaptonemal complex formation, which correlates with inefficient but existing nuclear rotations in *sas-4* and *asl* knockdowns. In contrast, in the absence of dynamic microtubules or Dynein motor, and thus, in the complete absence of nuclear rotations, pre-meiotic pairing, centromere clustering and synapsis between homologues are strongly affected.

SUN- and KASH-domain proteins Klaroid and Klarsicht are required for centromere dynamics, pairing and synapsis

SUN- and KASH-domain proteins are transmembrane proteins localizing at the inner and outer nuclear membranes respectively, and form bridges between the inside of the nucleus and the cytoplasmic cytoskeleton in a wide range of cells[40–43]. In *Drosophila*, two genes encode for SUN-domain proteins, Klaroid and Spag4, and two genes encode for KASH-domain proteins, Klarsicht and MSP-300 (refs 44–48). Spag4 is expressed specifically in male testis[45], whereas MSP-300 interacts with actin rather than microtubules[48,49]. We thus decided to investigate the function of *klaroid* (*koi*) and *klarsicht* (*klar*) during early female meiosis.

As previously published, both Klar and Koi exhibited a homogeneous perinuclear localization across all stages in germline and

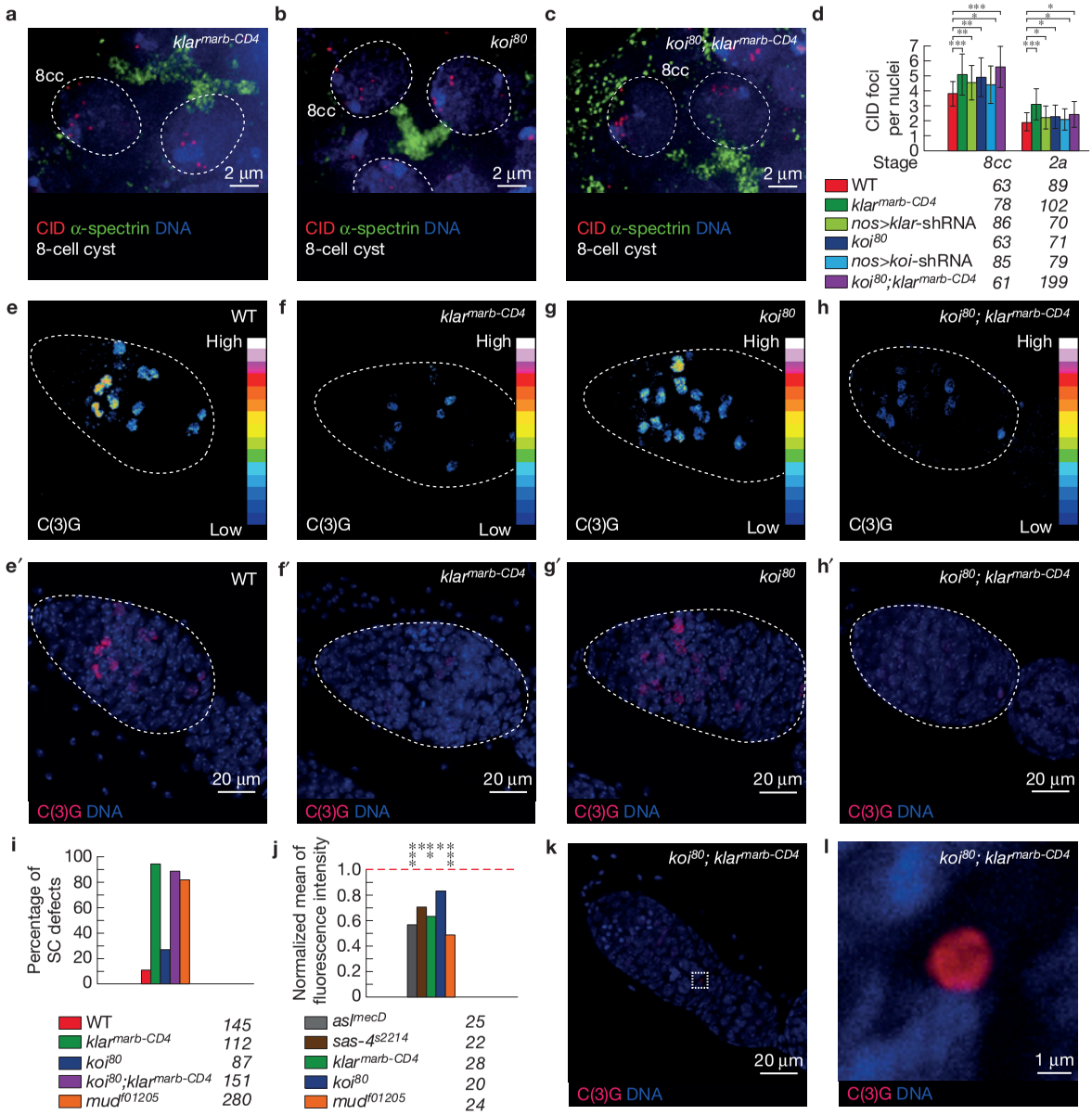

Figure 6 *klarsicht* and *klaroid* loss of function affects centromeric pairing in 8-cell cyst (8cc) and synaptonemal complex assembly in pachytene nuclei. (**a**–**c**) Projection of *Z*-sections obtained by deconvolution microscopy of a $klar^{marb\text{-}CD4}$ (**a**), koi^{80} (**b**) and koi^{80}; $klar^{marb\text{-}CD4}$ (**c**) fixed germarium stained for centromere (CID, red), fusome (α-spectrin, green), and DNA (DAPI, blue). Nuclei of 8-cell cysts are indicated by a dotted circle. (**d**) Developmental changes in the number of CID foci in 8-cell cyst nuclei and in pachytene nuclei in region 2a in wild-type, $klar^{marb\text{-}CD4}$, *nos*>*klar*_shRNA, koi^{80}, *nos*>*koi*_shRNA and koi^{80}; $klar^{marb\text{-}CD4}$ fixed germaria. The number of analysed cells (*n*) is indicated for each stage (data collected across 3 independent experiments for each genotype; mean ± s.d.; two-tailed Student's *t*-tests $^{*}P<5\times10^{-2}$, $^{**}P<5\times10^{-5}$, $^{***}P<5\times10^{-8}$). (**e**–**h′**) Projection of *Z*-sections obtained by confocal microscopy of a wild-type (**e**,**e′**), $klar^{marb\text{-}CD4}$ (**f**,**f′**), koi^{80} (**g**,**g′**) and koi^{80}; $klar^{marb\text{-}CD4}$ (**h**,**h′**) fixed germarium stained for synaptonemal complex (C(3)G, red). **e**–**h** correspond to 16-colour conversions of projections **e′**–**h′** respectively to better illustrate signal intensity differences (ImageJ: Image: Lookup tables: 16 colours). Germaria are indicated by a dotted line. (**i**) Changes in the percentage of germaria exhibiting synaptonemal complex (SC) defects in wild-type, $klar^{marb\text{-}CD4}$, koi^{80}, koi^{80}; $klar^{marb\text{-}CD4}$ and mud^{f01205} (khi2 tests: $klar^{marb\text{-}CD4}$, koi^{80}; $klar^{marb\text{-}CD4}$ and mud^{f01205} $P<5\times10^{-5}$). The number of analysed germaria (*n*) is indicated for each stage. Data collected across 3 independent experiments of each genotype. (**j**) Synaptonemal complex fluorescence intensity was quantified in $sas\text{-}4^{S2214}$, asl^{MecD}, $klar^{marb\text{-}CD4}$, koi^{80} and mud^{f01205} mutants. Each one was normalized to the intensity of wild-type controls (dotted red line equal to 1) introduced in the mutant preparation. The number of analysed germaria (*n* value) is indicated for each stage (data collected across 3 experiments; two-tailed Student's *t*-tests $^{*}P<5\times10^{-2}$, $^{**}P<5\times10^{-5}$, $^{***}P<5\times10^{-8}$). (**k**) Projection of *Z*-sections, obtained by confocal microscopy of a koi^{80}; $klar^{marb\text{-}CD4}$ fixed germarium stained for synaptonemal complex (C(3)G, red), and DNA (DAPI, blue). (**l**) A polycomplex from the corresponding outlined region in **j**.

somatic nuclei (Supplementary Fig. 4)[46]. However, in region 1 germ cells, both Klar and Koi formed dots at the NE (Fig. 5). Interestingly, these dots often co-localized or were in close proximity to centromeres in fixed and live ovaries (Fig. 5a–a‴,b and Supplementary Video 18). We observed this co-localization mostly in 8-cell cysts, but also in some 4-cell and 16-cell cysts (Supplementary Fig. 4).

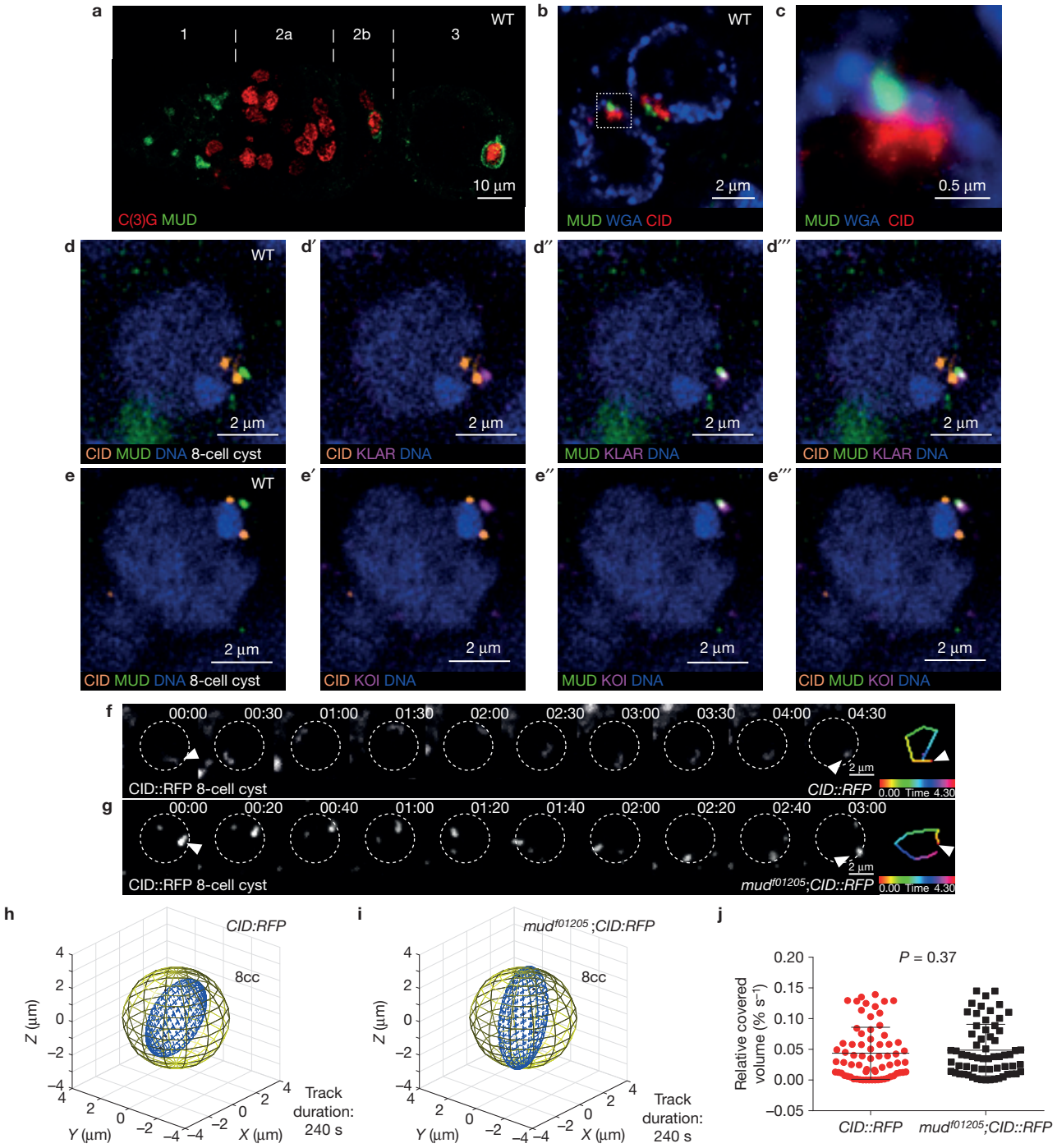

Figure 7 Mud associates with Klarsicht and Klaroid in 8-cell cysts close to centromeres, but is not required for chromosome movements. (**a**) Projection of *Z*-sections obtained by confocal microscopy of a wild-type fixed germarium stained for MUD (green) and synaptonemal complex (C(3)G, red). (**b**) Projection of *Z*-sections, obtained by confocal microscopy of a wild-type fixed germarium stained for MUD (green), the centromeres (CID, red) and the nuclear membrane (WGA, blue). (**c**) A close-up view of a CID–MUD association from the corresponding region outlined in **b**. (**d**–**d‴**) Projection of *Z*-sections obtained by deconvolution microscopy of a wild-type 8-cell cyst stained for centromeres (CID, orange), Mud (Mud, green), Klarsicht (Klar, magenta) and DNA (DAPI, blue). (**e**–**e‴**) Projection of *Z*-sections obtained by deconvolution microscopy of a wild-type 8-cell cyst stained for centromeres (CID, orange), Mud (Mud, green), Klaroid (Koi, magenta) and DNA (DAPI, blue). (**f**,**g**) *mud*^{f01205} mutation has little effect on CID foci dynamics in 8-cell cysts. Selected projections of a *CID–RFP* (**f**) and *mud*^{f01205}*; CID–RFP* (**g**) germarium showing a single 8-cell cyst nucleus over a 3-min time course (nuclear surface is indicated by a dotted circle in each image). The corresponding time-coloured tracking for one CID–RFP dot (arrowhead) is shown at the end of each time-lapse sequence. (**h**,**i**) Three-dimensional representations indicating the relative covered volume of one selected track for all time points of a *CID–RFP* (**h**) and a *mud*^{f01205}*; CID–RFP* (**i**) 8-cell cyst (8cc) nucleus. The ellipsoid is arbitrarily centred into a sphere representing the nuclear volume (gold sphere) of an 8-cell cyst stage. (**j**) Distributions of the relative covered volume per second for centromeric foci in *CID–RFP* and *mud*^{f01205}; *CID–RFP* 8-cell cyst nuclei. Mann–Whitney *U*-test comparing *CID–RFP* with *mud*^{f01205}; *CID–RFP* 8-cell cyst nuclei ($P = 0.37$) (mean ± s.d., CID::RFP: $n = 70$ centromeric foci; collected across 3 independent experiments, *mud*^{f01205}: $n = 63$ centromeric foci/3 independent experiments).

In 8-cell cysts mutant for null alleles of *klaroid* and *klarsicht*, koi^{80} and $klar^{marb\text{-}CD4}$ respectively[44,50], centromere motions were reduced and the relative covered volume per second was also significantly decreased (Fig. 5c–g and Supplementary Videos 19 and 20). Some centromere foci still exhibited circular movements but at a much lower speed; thus, the volume covered per second was low. These movements were more affected in $klar^{marb\text{-}CD4}$ than in koi^{80} mutant germ cells (Fig. 5g and Supplementary Fig. 5).

We then investigated the effects of *klarsicht* and *klaroid* loss of function on pre-meiotic centromere pairing, clustering and synapsis. Centromere pairing was significantly affected in $klar^{marb\text{-}CD4}$, koi^{80} and $klar^{marb\text{-}CD4}$; koi^{80} double-mutant ovaries (Fig. 6a–d, and RNAi in Supplementary Table 1). Clustering of centromeres in region 2a pachytene nuclei was also disrupted, but much less markedly (Fig. 6d). Most $klar^{marb\text{-}CD4}$ and $klar^{marb\text{-}CD4}$; koi^{80} mutant ovaries had a reduced level of synaptonemal complex, indicating defects in synapsis (Fig. 6f,h–j). In contrast, most pachytene nuclei mutant for koi^{80} showed a normal synaptonemal complex (Fig. 6g,i,j). In addition, in some $klar^{marb\text{-}CD4}$; koi^{80} double-mutant germaria, large aggregates of synaptonemal complex were observed instead of the typical filamentous thread-like structure (7.3%, $n = 151$, Fig. 6j,k and Supplementary Fig. 6). These aggregates were reminiscent of the polycomplexes described previously[51].

Overall, we conclude that the KASH-domain protein Klarsicht and the SUN-domain protein Klaroid are essential for centromere motions and pairing, and also play an important function in synaptonemal complex assembly.

The Dynein-interacting protein Mud co-localizes with Klarsicht/Klaroid and is required for synapsis between homologues

Next, we searched for proteins directly interacting with Dynein and the nuclear envelope, which could play a role during meiosis. We focused on Mud (Mushroom body defect), the *Drosophila* homologue of NuMA, for several reasons: vertebrate NuMA is known to interact directly with Dynein to assemble the mitotic spindle, and its *Drosophila* and *C. elegans* homologues interact with Dynein to position the spindle in neuroblasts and the one-cell stage embryo[52–56]; *mud* null alleles are viable but females are sterile and males are fertile, indicating a specific requirement for *mud* in female germ cell development; Mud is an essential component of the meiosis II spindle in *Drosophila* oocyte[57]; and Mud is expressed in the germarium and localizes to the nuclear envelope[57] (Figs 7a and 8f).

In addition to this localization, we noticed dots of Mud on the cytoplasmic side of the NE that were precisely juxtaposed to centromeres (Fig. 7b,c), and could co-localize with Klarsicht and Klaroid (Fig. 7d–e‴). We then analysed germaria mutant for *mud* to investigate a potential function in regions 1 and 2. Live imaging showed that the mud^{f01205} mutation did not disturb significantly centromere dynamics (Fig. 7g,i,j and Supplementary Videos 21 and 22). Centromere pairing and clustering were only slightly affected in mud^{f01205} germaria (Fig. 8b,c). However, we detected significant genetic interactions between *mud* and both *klarsicht* and *klaroid* for centromere pairing, but not for centromere clustering (Fig. 8c and Supplementary Tables 2 and 3).

Next, we examined the assembly of the synaptonemal complex in mud^{f01205} mutant germaria by analysing the localization of C(3)G. We found that 82% of mutant germaria and around 90% of germaria expressing *mud*_shRNA exhibited reduced fluorescence ranging from 30 to 40% for the shRNA and 50% for mud^{f01205} (Figs 8d,e and 6i,j; and Supplementary Fig. 7). Strikingly, 16% of mud^{f01205} germaria formed polycomplexes instead of thread-like synaptonemal complexes (Supplementary Fig. 5). These polycomplexes could be found as early as region 2a and were still visible in later stages of oogenesis (Fig. 8h,i). The presence of polycomplexes correlated with an absence of nuclear envelope marked by Lamin and by Lectin (Fig. 8g,h and Supplementary Fig. 8). DAPI (4′,6-diamidino-2-phenylindole) staining also revealed that DNA was diffused in the oocyte cytoplasm (Fig. 8h,i). Despite this nuclear phenotype, mutant oocytes were correctly determined and polarized, and grew properly into late-stage egg chambers (Fig. 8i).

We examined in more detail the structure of polycomplexes by super-resolution microscopy using antibodies against C(3)G and Corona (Cona), which are transverse filaments and central element components of the synaptonemal complex, respectively, and required for synaptonemal complex formation[58,59]. In wild-type pachytene nuclei, the central element protein Cona localized as a single line between two threads of C(3)G labelling the edges of the transverse filament, as predicted from previous studies[59] (Fig. 8j–j′). In mud^{f01205} polycomplexes, we could also distinguish alternate threads of Cona and C(3)G, indicating that the polycomplexes were not simple aggregates of synaptonemal complex components as observed with regular confocal microscopy (Fig. 8k–k′). Overall, these data suggest that Mud played a minor role in centromere dynamics and pairing, but is required for the integrity of the nuclear membrane and the assembly of the synaptonemal complex.

DISCUSSION

Rotations of nuclei have been described previously in somatic cells; their function remains however unclear[60–63]. In germ cells, meiotic chromosome movements are thought to be required for homologue pairing, removing chromosome entanglements, promoting maturation of recombination intermediates, or for assessing chromosome homology before synapsis, in different model organisms[64,65]. In *Drosophila*, we found a high temporal correlation between nuclear rotations and chromosome pairing occurring mainly in 8-cell cysts. Our work uncovered a second interesting correlation between the speed of nuclear rotation and the degree of centromere pairing and clustering. Indeed, mutations in *klaroid* affected the least nuclear rotations and disrupted the least centromere associations and synapsis. Rotations were slowed down more significantly in *klarsicht*, *sas-4* and *asl* mutant germ cells. Accordingly, we observed strong defects in the initial pairing of centromeres and in synaptonemal complex formation. Finally, nuclear rotations were completely abolished in the absence of Dynein or dynamic microtubules. In *dynein* mutant germ cells, we could distinguish an average of six centromeres during pre-meiotic pairing, which is higher than any mutants we have tested previously, including null alleles of *c(3)G* (ref. 23). Similarly, we counted five centromeres on average during clustering in region 2a, a mutant phenotype that is comparable to the strongest *ord* or *c(3)G* mutations (lateral and central elements

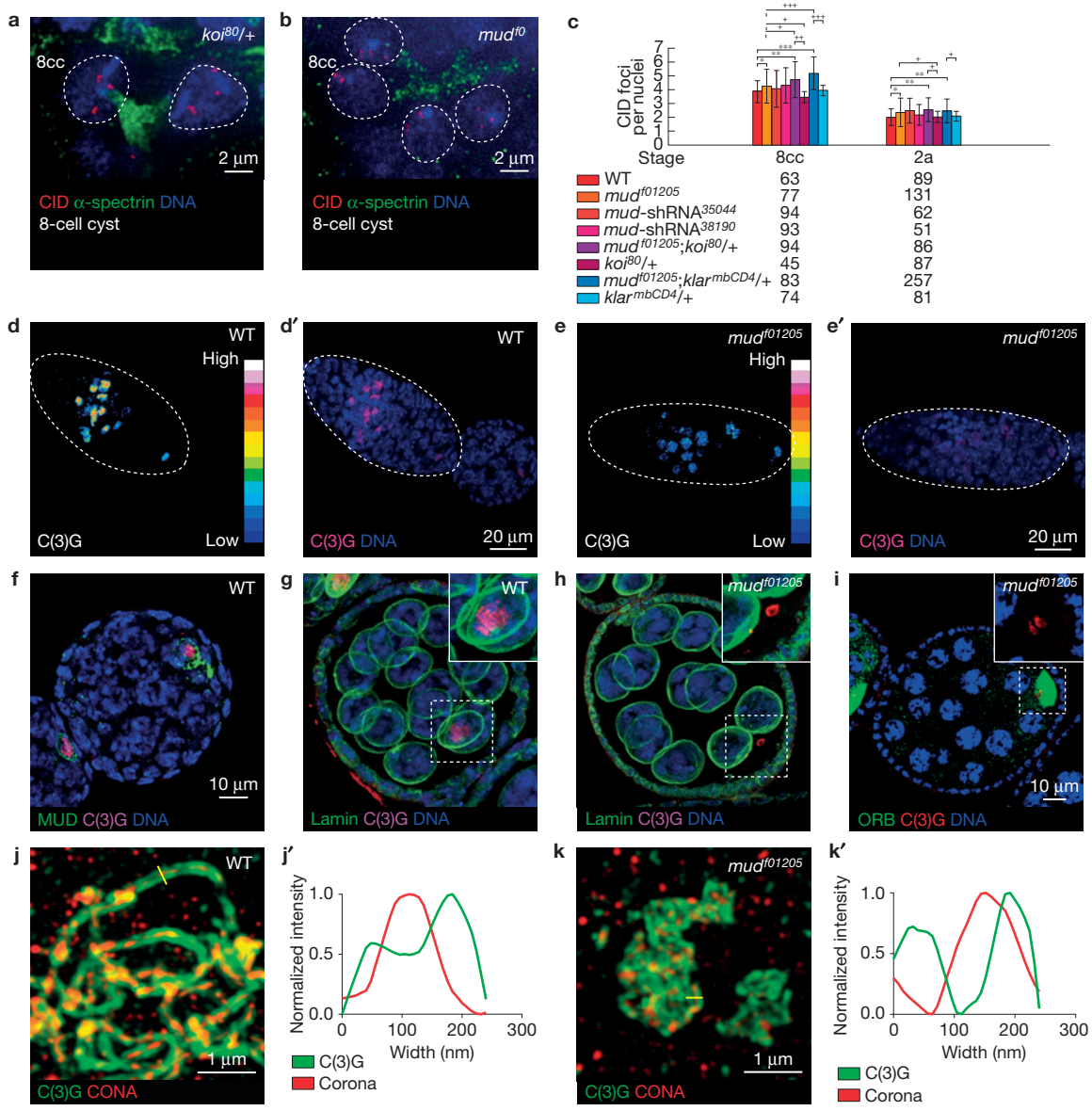

Figure 8 *mud* plays a minor role in centromere pairing in the 8-cell cyst (8cc) but is required to maintain the nuclear envelope integrity and for the assembly of the synaptonemal complex. (**a**,**b**) *Z*-projections of a $koi^{80}/+$ (**a**) and mud^{f01205} (**b**) fixed germarium stained for centromeres (CID, red), fusome (α-spectrin, green), and DNA (DAPI, blue). Nuclei of an 8-cell cyst with a branched fusome are shown. (**c**) Developmental changes in the number of CID foci for the 8-cell cyst cell stage and in pachytene nuclei in region 2a in wild-type and different mutant and shRNA conditions. The number of analysed cells (*n* value) is indicated for each stage (data collected across 3 independent experiments for each genotype; error bars are mean ± s.d.; two-tailed Student's *t*-tests: $^{*}P < 5 \times 10^{-2}$, $^{**}P < 5 \times 10^{-5}$, $^{***}P < 5 \times 10^{-8}$; two-tailed Student's *t*-tests with Bonferroni correction after ANOVA: $^{+}P < 1.67 \times 10^{-2}$, $^{++}P < 1.67 \times 10^{-5}$, $^{+++}P < 1.67 \times 10^{-8}$). (**d**–**e**′) *Z*-projections of a wild-type (**d**,**d**′) and mud^{f01205} (**e**,**e**′) fixed germarium stained for synaptonemal complex (C(3)G, red). **d** and **e** correspond to 16-colour conversions of projections **d**′ and **e**′ respectively to better illustrate signal intensity differences. (**f**) *Z*-projections of wild-type stage 3 egg chamber stained for MUD in green, C(3)G in red and DNA. (**g**,**h**) *Z*-projections of wild-type (**g**) and mud^{f01205} (**h**) stage 3 egg chambers stained for C(3)G in red, the nuclear membrane (lamin, green), and DNA. mud^{f01205} mutant oocytes showing polycomplexes also have diffused DNA and their NE has collapsed. (**i**) *Z*-projections of wild-type stage 3 egg chamber stained for C(3)G in red, Orb in green and DNA. Oocytes with polycomplexes in mud^{f01205} mutants still exhibit polarized localization of Orb. (**j**–**k**′) *Z*-projections obtained by structured illumination microscopy of carboxy-terminal C(3)G (green) and Cona (red) on pachytene nuclei from the wild type and polycomplexes from mud^{f01205}. (**j**) In wild-type pachytene nuclei, Cona localizes between the two threads of C(3)G. (**j**′) Line profiles plot the normalized intensity for Cona (red) and C(3)G (green) from **j**. The Cona peak is seen between the two parallel peaks of C(3)G. (**k**) Structured illumination microscopy of polycomplexes in a mud^{f01205} germarium showed that there is still an alternate although disorganized structure where Cona localizes between the two threads of C(3)G. (**k**′) Line profiles from panel **k** confirm that in polycomplexes Cona still localizes between the two threads of C(3)G.

of synaptonemal complex respectively)[10,11]. Nuclear rotations thus play an important role in homologue chromosome pairing and synaptonemal complex formation.

We found that microtubules could be nucleated from the fusome, the nuclear envelope and the centrosome in region 1 germ cells. On the basis of these observations and our centrosome

mutant analysis, we can speculate that the whip-like movements of microtubules could be the main forces creating cytoplasmic flows, as observed in many biological systems and demonstrated theoretically[66]. In addition, microtubules nucleated by the centrosomes could also push on the nucleus and the cell membrane, which could bias nuclear movement towards one direction of rotation as proposed for the migration of this same oocyte nucleus later on during oogenesis[67]. These two forces depend on microtubules and dynein, and would act redundantly for efficient and unidirectional nuclear rotations.

However, even in the absence of dynamic microtubules, centromeres ended up paired, albeit much later in region 2b (Supplementary Fig. 3). Synapsis, on the other hand, was completely disrupted. We thus believe that, as in yeast and worms, these movements are there to facilitate pairing, synapsis or recombination, but that at least chromosome pairing could occur slowly without motions by redundant mechanisms. In flies, Spag4 is a second SUN-domain protein, but it is only expressed in male testis and is thus not likely to play a role during oogenesis[45]. There is also a second KASH-domain protein called MSP-300/Nesprin, which interacts with the actin cytoskeleton[48,49]. In the absence of microtubules, nuclei were not 'rolling' anymore; however, they still showed some back and forth 'rocking' movements. It will be interesting to investigate whether MSP300/Nesprin and the actin cytoskeleton are involved in these rocking movements[18,31].

We found that although *mud* mutant ovaries showed only mild defects in centromere dynamics, we uncovered significant genetic interactions with *klaroid* and *klarsicht* in this same process. Striking features of Mud in our study were its co-localization with centromeres in interphasic germline cysts and the formation of polycomplexes in *mud* mutant cysts. The formation of polycomplexes was associated with a lack of nuclear membrane and diffused DNA in the cytoplasm, suggesting that Mud is required to maintain nuclear envelope integrity. We propose that the disappearance of the NE in *mud* cysts is the primary defect leading first to the de-localization of DNA into the cytoplasm and then the formation of polycomplexes. Polycomplexes could thus be the result of self-assembly of synaptonemal complex components polymerizing in the absence of chromatin. We also observed polycomplexes in *klaroid* and *klarsicht* mutants although at a lower penetrance than in *mud* mutants. Interestingly, large distortions of the NE were also observed in muscle cell nuclei mutant for *unc-84*, which encodes a *C. elegans* SUN protein[68]. These deformations were particularly strong in these cells, because muscle cell nuclei are subjected to mechanical stress. It is likely that rolling nuclei of 8-cell cysts are also exposed to some mechanical forces. Klarsicht, Klaroid and Mud may all participate in maintaining the integrity of the nuclear envelope in these conditions. In their absence, the NE is weakened and cannot resist mechanical forces, which also leads to synaptonemal complex assembly defects. In the most extreme cases the NE completely disappears causing the formation of polycomplexes. Interestingly, Mud initially localizes at the NE of all germline cells in region 1, but then becomes localized only to the cells remaining in meiosis in region 2a, and finally only specifically at the NE of the oocyte (Figs 7a and 8f). This may hint that the meiotic nucleus is subjected to specific mechanical forces during oogenesis. □

METHODS

Methods and any associated references are available in the online version of the paper.

Note: Supplementary Information is available in the online version of the paper

ACKNOWLEDGEMENTS

We wish to thank F. Llense for observing that Mud co-localized with centromeres and E. Heard for suggesting 'rolling' nuclei. We are grateful to S. Roth (University of Cologne, Germany), M. Welte, J. Fischer and the Bloomington Stock centre for flies and reagents. We acknowledge great technical support from the PICT@BDD imaging platform. This work was supported by the European Research Council (ERC EPIGENETIX No 250367). N.C. is supported by Institut Curie, FRM post-doctoral fellowship (SPF20111223331) and DEEP LabEx; T.R. is supported by an FRM Ingenieur Fellowship (no ING20140129247); the J.-R.H. laboratory is funded by CNRS, Ville de Paris, ANR and FSER (Schlumberger).

AUTHOR CONTRIBUTIONS

N.C., T.R. and J.-R.H conceived and designed the experiments. N.C., T.R. and M.A. performed the experiments. N.C., T.R. and J.-R.H. analysed the data. I.B. conceived and performed centromere correlation analysis. T.P. performed SIM microscopy. J.-R.H. and N.C. wrote the paper.

COMPETING FINANCIAL INTERESTS

The authors declare no competing financial interests.

Published online at http://dx.doi.org/10.1038/ncb3249
Reprints and permissions information is available online at www.nature.com/reprints

1. Bhalla, N. & Dernburg, A. F. Prelude to a division. *Annu. Rev. Cell Dev. Biol.* **24,** 397–424 (2008).
2. Lake, C. M. & Hawley, R. S. The molecular control of meiotic chromosomal behavior: events in early meiotic prophase in *Drosophila* oocytes. *Annu. Rev. Physiol.* **74,** 425–451 (2012).
3. Page, S. L. & Hawley, R. S. The genetics and molecular biology of the synaptonemal complex. *Annu. Rev. Cell Dev. Biol.* **20,** 525–558 (2004).
4. Obeso, D., Pezza, R. J. & Dawson, D. Couples, pairs, and clusters: mechanisms and implications of centromere associations in meiosis. *Chromosoma* **123,** 43–55 (2014).
5. Tsai, J. H. & McKee, B. D. Homologous pairing and the role of pairing centers in meiosis. *J. Cell Sci.* **124,** 1955–1963 (2011).
6. Gerton, J. L. & Hawley, R. S. Homologous chromosome interactions in meiosis: diversity amidst conservation. *Nat. Rev. Genet.* **6,** 477–487 (2005).
7. Boateng, K. A., Bellani, M. A., Gregoretti, I. V., Pratto, F. & Camerini-Otero, R. D. Homologous pairing preceding SPO11-mediated double-strand breaks in mice. *Dev. Cell* **24,** 196–205 (2013).
8. Brown, P. W. *et al.* Meiotic synapsis proceeds from a limited number of subtelomeric sites in the human male. *Am. J. Hum. Genet.* **77,** 556–566 (2005).
9. MacQueen, A. J. *et al.* Chromosome sites play dual roles to establish homologous synapsis during meiosis in *C. elegans*. *Cell* **123,** 1037–1050 (2005).
10. Takeo, S., Lake, C. M., Morais-de-Sa, E., Sunkel, C. E. & Hawley, R. S. Synaptonemal complex-dependent centromeric clustering and the initiation of synapsis in *Drosophila* oocytes. *Curr. Biol.* **21,** 1845–1851 (2011).
11. Tanneti, N. S., Landy, K., Joyce, E. F. & McKim, K. S. A pathway for synapsis initiation during zygotene in *Drosophila* oocytes. *Curr. Biol.* **21,** 1852–1857 (2011).
12. Scherthan, H. A bouquet makes ends meet. *Nat. Rev. Mol. Cell Biol.* **2,** 621–627 (2001).
13. Zickler, D. From early homologue recognition to synaptonemal complex formation. *Chromosoma* **115,** 158–174 (2006).
14. Zickler, D. & Kleckner, N. The leptotene–zygotene transition of meiosis. *Annu. Rev. Genet.* **32,** 619–697 (1998).
15. Baudrimont, A. *et al.* Leptotene/zygotene chromosome movement via the SUN/KASH protein bridge in *Caenorhabditis elegans*. *PLoS Genet.* **6,** e1001219 (2010).
16. Shibuya, H., Ishiguro, K. & Watanabe, Y. The TRF1-binding protein TERB1 promotes chromosome movement and telomere rigidity in meiosis. *Nat. Cell Biol.* **16,** 145–156 (2014).
17. Wynne, D. J., Rog, O., Carlton, P. M. & Dernburg, A. F. Dynein-dependent processive chromosome motions promote homologous pairing in *C. elegans* meiosis. *J. Cell Biol.* **196,** 47–64 (2012).
18. Shibuya, H., Morimoto, A. & Watanabe, Y. The dissection of meiotic chromosome movement in mice using an *in vivo* electroporation technique. *PLoS Genet.* **10,** e1004821 (2014).
19. Lee, C. Y. *et al.* Mechanism and regulation of rapid telomere prophase movements in mouse meiotic chromosomes. *Cell Rep.* **11,** 551–563 (2015).
20. Ding, D. Q., Chikashige, Y., Haraguchi, T. & Hiraoka, Y. Oscillatory nuclear movement in fission yeast meiotic prophase is driven by astral microtubules, as revealed by continuous observation of chromosomes and microtubules in living cells. *J. Cell Sci.* **111,** 701–712 (1998).

21. Trelles-Sticken, E., Adelfalk, C., Loidl, J. & Scherthan, H. Meiotic telomere clustering requires actin for its formation and cohesin for its resolution. *J. Cell Biol.* **170,** 213–223 (2005).
22. Cahoon, C. K. & Hawley, R. S. Flies get a head start on meiosis. *PLoS Genet.* **9,** e1004051 (2013).
23. Christophorou, N., Rubin, T. & Huynh, J. R. Synaptonemal complex components promote centromere pairing in pre-meiotic germ cells. *PLoS Genet.* **9,** e1004012 (2013).
24. Joyce, E. F., Apostolopoulos, N., Beliveau, B. J. & Wu, C. T. Germline progenitors escape the widespread phenomenon of homolog pairing during *Drosophila* development. *PLoS Genet.* **9,** e1004013 (2013).
25. Huynh, J. R. & St Johnston, D. The origin of asymmetry: early polarisation of the *Drosophila* germline cyst and oocyte. *Curr. Biol.* **14,** R438–R449 (2004).
26. Mathieu, J. *et al.* Aurora B and cyclin B have opposite effects on the timing of cytokinesis abscission in *Drosophila* germ cells and in vertebrate somatic cells. *Dev. Cell* **26,** 250–265 (2013).
27. Fichelson, P. *et al.* Live-imaging of single stem cells within their niche reveals that a U3snoRNP component segregates asymmetrically and is required for self-renewal in *Drosophila*. *Nat. Cell Biol.* **11,** 685–693 (2009).
28. Huynh, J. R., Shulman, J. M., Benton, R. & St Johnston, D. PAR-1 is required for the maintenance of oocyte fate in *Drosophila*. *Development* **128,** 1201–1209 (2001).
29. Schuh, M., Lehner, C. F. & Heidmann, S. Incorporation of *Drosophila* CID/CENP-A and CENP-C into centromeres during early embryonic anaphase. *Curr. Biol.* **17,** 237–243 (2007).
30. Yoshida, M. *et al.* Microtubule-organizing center formation at telomeres induces meiotic telomere clustering. *J. Cell Biol.* **200,** 385–395 (2013).
31. Sheehan, M. & Pawlowski, W. P. Live imaging of rapid chromosome movements in meiotic prophase I in maize. *Proc. Natl Acad. Sci. USA* **106,** 20989–20994 (2009).
32. Bolivar, J. *et al.* Centrosome migration into the *Drosophila* oocyte is independent of BicD and egl, and of the organisation of the microtubule cytoskeleton. *Development* **128,** 1889–1897 (2001).
33. Grieder, N. C., de Cuevas, M. & Spradling, A. C. The fusome organizes the microtubule network during oocyte differentiation in *Drosophila*. *Development* **127,** 4253–4264 (2000).
34. Theurkauf, W. E. & Hazelrigg, T. I. *In vivo* analyses of cytoplasmic transport and cytoskeletal organization during *Drosophila* oogenesis: characterization of a multi-step anterior localization pathway. *Development* **125,** 3655–3666 (1998).
35. Mahowald, A. P. & Strassheim, J. M. Intercellular migration of centrioles in the germarium of *Drosophila melanogaster*. An electron microscopic study. *J. Cell Biol.* **45,** 306–320 (1970).
36. Stevens, N. R., Raposo, A. A., Basto, R., St Johnston, D. & Raff, J. W. From stem cell to embryo without centrioles. *Curr. Biol.* **17,** 1498–1503 (2007).
37. Basto, R. *et al.* Flies without centrioles. *Cell* **125,** 1375–1386 (2006).
38. Blachon, S. *et al. Drosophila* asterless and vertebrate Cep152 are orthologs essential for centriole duplication. *Genetics* **180,** 2081–2094 (2008).
39. Ni, J. Q. *et al.* A genome-scale shRNA resource for transgenic RNAi in *Drosophila*. *Nat. Methods* **8,** 405–407 (2011).
40. Hiraoka, Y. & Dernburg, A. F. The SUN rises on meiotic chromosome dynamics. *Dev. Cell* **17,** 598–605 (2009).
41. Rothballer, A. & Kutay, U. The diverse functional LINCs of the nuclear envelope to the cytoskeleton and chromatin. *Chromosoma* **122,** 415–429 (2013).
42. Starr, D. A. & Fridolfsson, H. N. Interactions between nuclei and the cytoskeleton are mediated by SUN-KASH nuclear-envelope bridges. *Annu. Rev. Cell Dev. Biol.* **26,** 421–444 (2010).
43. Tapley, E. C. & Starr, D. A. Connecting the nucleus to the cytoskeleton by SUN-KASH bridges across the nuclear envelope. *Curr. Opin. Cell Biol.* **25,** 57–62 (2013).
44. Kracklauer, M. P., Banks, S. M., Xie, X., Wu, Y. & Fischer, J. A. *Drosophila* klaroid encodes a SUN domain protein required for Klarsicht localization to the nuclear envelope and nuclear migration in the eye. *Fly* **1,** 75–85 (2007).
45. Kracklauer, M. P. *et al.* The *Drosophila* SUN protein Spag4 cooperates with the coiled-coil protein Yuri Gagarin to maintain association of the basal body and spermatid nucleus. *J. Cell Sci.* **123,** 2763–2772 (2010).
46. Technau, M. & Roth, S. The *Drosophila* KASH domain proteins Msp-300 and Klarsicht and the SUN domain protein Klaroid have no essential function during oogenesis. *Fly* **2,** 82–91 (2008).
47. Fischer-Vize, J. A. & Mosley, K. L. Marbles mutants: uncoupling cell determination and nuclear migration in the developing *Drosophila* eye. *Development* **120,** 2609–2618 (1994).
48. Volk, T. A new member of the spectrin superfamily may participate in the formation of embryonic muscle attachments in *Drosophila*. *Development* **116,** 721–730 (1992).
49. Yu, J. *et al.* The KASH domain protein MSP-300 plays an essential role in nuclear anchoring during *Drosophila* oogenesis. *Dev. Biol.* **289,** 336–345 (2006).
50. Mosley-Bishop, K. L., Li, Q., Patterson, L. & Fischer, J. A. Molecular analysis of the klarsicht gene and its role in nuclear migration within differentiating cells of the *Drosophila* eye. *Curr. Biol.* **9,** 1211–1220 (1999).
51. Jeffress, J. K. *et al.* The formation of the central element of the synaptonemal complex may occur by multiple mechanisms: the roles of the N- and C-terminal domains of the *Drosophila* C(3)G protein in mediating synapsis and recombination. *Genetics* **177,** 2445–2456 (2007).
52. Bowman, S. K., Neumuller, R. A., Novatchkova, M., Du, Q. & Knoblich, J. A. The *Drosophila* NuMA homolog Mud regulates spindle orientation in asymmetric cell division. *Dev. Cell* **10,** 731–742 (2006).
53. Izumi, Y., Ohta, N., Hisata, K., Raabe, T. & Matsuzaki, F. *Drosophila* Pins-binding protein Mud regulates spindle-polarity coupling and centrosome organization. *Nat. Cell Biol.* **8,** 586–593 (2006).
54. Merdes, A., Ramyar, K., Vechio, J. D. & Cleveland, D. W. A complex of NuMA and cytoplasmic dynein is essential for mitotic spindle assembly. *Cell* **87,** 447–458 (1996).
55. Nguyen-Ngoc, T., Afshar, K. & Gonczy, P. Coupling of cortical dynein and G alpha proteins mediates spindle positioning in *Caenorhabditis elegans*. *Nat. Cell Biol.* **9,** 1294–1302 (2007).
56. Siller, K. H., Cabernard, C. & Doe, C. Q. The NuMA-related Mud protein binds Pins and regulates spindle orientation in *Drosophila* neuroblasts. *Nat. Cell Biol.* **8,** 594–600 (2006).
57. Yu, J. X., Guan, Z. & Nash, H. A. The mushroom body defect gene product is an essential component of the meiosis II spindle apparatus in *Drosophila* oocytes. *Genetics* **173,** 243–253 (2006).
58. Page, S. L. & Hawley, R. S. c(3)G encodes a *Drosophila* synaptonemal complex protein. *Genes Dev.* **15,** 3130–3143 (2001).
59. Page, S. L. *et al.* Corona is required for higher-order assembly of transverse filaments into full-length synaptonemal complex in *Drosophila* oocytes. *PLoS Genet.* **4,** e1000194 (2008).
60. Paddock, S. W. & Albrecht-Buehler, G. The degree of coupling of nuclear rotation in binucleate 3T3 cells. *Exp. Cell Res.* **166,** 113–126 (1986).
61. Paddock, S. W. & Albrecht-Buehler, G. Distribution of microfilament bundles during rotation of the nucleus in 3T3 cells treated with monensin. *Exp. Cell Res.* **163,** 525–538 (1986).
62. Pomerat, C. M. Rotating nuclei in tissue cultures of adult human nasal mucosa. *Exp. Cell Res.* **5,** 191–196 (1953).
63. Szikora, S., Gaspar, I. & Szabad, J. 'Poking' microtubules bring about nuclear wriggling to position nuclei. *J. Cell Sci.* **126,** 254–262 (2013).
64. Koszul, R. & Kleckner, N. Dynamic chromosome movements during meiosis: a way to eliminate unwanted connections? *Trends Cell Biol.* **19,** 716–724 (2009).
65. Woglar, A. & Jantsch, V. Chromosome movement in meiosis I prophase of Caenorhabditis elegans. *Chromosoma* **123,** 15–24 (2014).
66. Sanchez, T., Chen, D. T., DeCamp, S. J., Heymann, M. & Dogic, Z. Spontaneous motion in hierarchically assembled active matter. *Nature* **491,** 431–434 (2012).
67. Zhao, T., Graham, O. S., Raposo, A. & St Johnston, D. Growing microtubules push the oocyte nucleus to polarize the *Drosophila* dorsal–ventral axis. *Science* **336,** 999–1003 (2012).
68. Cain, N. E., Tapley, E. C., McDonald, K. L., Cain, B. M. & Starr, D. A. The SUN protein UNC-84 is required only in force-bearing cells to maintain nuclear envelope architecture. *J. Cell Biol.* **206,** 163–172 (2014).

DOI: 10.1038/ncb3249

METHODS

Fly stocks and genetics. For all experiments on fixed and live germaria the following strains were used: w^{1118} was used as the wild-type strain when assaying centromere pairing and clustering and y^1w^{1118} hs-Flp; FRT82B::GFP as the wild-type strain when assaying synapsis. For testing mutants, the following strains were used: w^*; $sas\text{-}4^{s2214}$ (ref. 37), asl^{mecD} (ref. 38), $koi^{HRKO80.w}$ (refs 51,58), $klar^{mCD4}$ (ref. 59), w^{1118}, mud^{f01205} (ref. 69), $Dhc64c^{3\text{-}2}/Dhc64c^{6\text{-}12}$ (ref. 70). For shRNAs the following lines were used: UASp::Trip white (Bloomington: 35573); UASp::Trip Dhc64c (Bloomington: 36698 and 36583); UASp::Trip sas-4 (Bloomington: 35049); UASp::Trip asl (Bloomington: 38220); UASp::Trip klar (Bloomington: 36721); UASp::Trip koi (Bloomington: 40924); UASp::Trip mud (Bloomington: 38190 and 35044) (ref. 39). Also, for experiments on live germaria CID::RFP/+ (ref. 29); *nos*-Gal4/UASp::Par1:GFP/+ (fusome marker gift from D. St Johnston, University of Cambridge, UK); $w[^*]$, $P\{w[+mC] = $ GFP-Nup107.K$\}$13.2.1; wg[Sp-1]/CyO (Bloomington: 35513); pUASp-GFP:KASH/CyO (ref. 46); w[1118]; $P\{w[+mC]=$PTT-GA$\}$ Jupiter[G00147] (Bloomington: 6836) and $P\{$Ubi-YFP-asl.FL$\}$ were used.

Immunohistochemistry. For immunostaining, ovaries were dissected in PBS, fixed in 4%PFA–PEPS, permeabilized in PBT (0,2%Triton) for 30 min, left overnight with primary antibodies in PBS at 4 °C, washed 4 × 30 min in PBS, left with secondary antibody for 2 h at room temperature, washed 4 × 30 min in PBS where DAPI (1:500) was added during the last wash and mounted in Cityfluor. We used the following primary antibodies: mouse anti-C(3)G 1A8-1G2 (1:500), rabbit anti-C(3)G (1:1,000) and guinea pig anti-Cona (1:500) (gifts from S. Hawley, Stowers Institute, USA), rat anti-Cid (1:1,000) (gift from C. E. Sunkel, Universidade do Porto, Portugal), rabbit anti-αSpectrin (1:1,000) (gift from R. Dubreuil, University of Chicago, USA) to label the fusome and identify the cyst stages, rabbit anti-Mud (1:500; ref. 57), rat anti-Klaroid (1:200), guinea pig anti-Klarsicht (1:200) (gifts from M. Welte, University of Rochester, USA and J. Fischer, University of Texas, USA); mouse anti-Orb (1:500) (4H8, DSHB); mouse anti-Lamin (1:500) (ADL84.12, DSHB). Secondary antibodies conjugated with Cy3, Cy5 and FITC (Jackson laboratories) were used at 1:200. For lectin staining WGA conjugated to Alexa 488 was used (1:500).

Colcemid treatments. Colcemid was added to the fly medium at a concentration of 0.2 mg ml^{-1} diluted in saccharose 1% and added to dry yeast. To assay pairing and clustering of centromeres, long-term drug treatments lasted 48 h. Freshly prepared drug was added every 12 h. For live imaging, adult flies were fed for four hours with the colcemid-containing food. Ovaries were dissected as above and live imaging was performed as described below. Colcemid was inactivated with a brief ultraviolet pulse (5 s) using an inverted spinning-disc confocal microscope (Roper/Nikon). Flies expressing CID:RFP and Jupiter:GFP to see the microtubules were used as control flies to confirm the colcemid inactivation after the ultraviolet pulse.

Image acquisition and data analysis. Deconvolution microscopy images of fixed germaria were collected under a DeltaVision deconvolution microscope system (Applied Precision) equipped with an Olympus 1670 inverted microscope and a CoolSNAP HQ camera (Photometrics). All images were acquired with the PlanApo 60×/1.42 oil objective lens with ×1.5 auxiliary magnification at 0.2 µm intervals along the z axis and deconvolved using the softWoRx v.3.5.1 software (Applied Precision). Confocal images of fixed germaria were collected under a Zeiss LSM 700 NLO confocal. All images were acquired with a PlanApo 63×/1.40 oil objective at 0.6 µm intervals along the z axis and operated by ZEN 2012 software.

When structured illumination was performed we used a rotary-stage OMX v3 system (Applied Precision—GE Healthcare), equipped with 3 EMCCD, Evolve cameras (Photometrics). Signals from all channels were realigned using fluorescent beads before each session of image acquisition. Registration was done using UnwarpJ in ImageJ (W. S. Rasband). All images were acquired with a PlanApo 100×/1.4 oil objective at 125 nm intervals along the z axis. Pixel size is 40 nm along the xy axis after reconstruction.

The length of the synaptonemal complex was measured from deconvolution microscopy images with a macro on ImageJ designed by O. Leroy from the BDD imaging facility.

Fluorescence quantification and normalization was performed on confocal images. In brief, from each slide preparation, pictures of C(3)G staining of mutant or shRNA germaria and control germaria (GFP+) were taken under exactly the same settings (exposure, image size, bit depth, acquisition speed and so on). Fluorescence emitted per germarium was quantified and a mean ± s.d. was calculated. Finally the mean fluorescence of mutant germaria was normalized to the mean of fluorescence of control germaria. In the case of *sas-4* clones, fluorescence from individual nuclei was quantified.

For live imaging, ovaries were dissected in oil (10S, Voltalef, VWR). The muscular sheath around each ovariole was removed and germaria were made to stick to coverslips in oil.

Videos were collected with an inverted spinning-disc confocal microscope (Roper/Nikon) operated by Metamorph on an inverted NikonEclipse Ti microscope coupled to an Evolve EMCCD camera (Photometrics) or a CoolSNAP HQ2 camera (Photometrics) for colcemid experiments and a temperature control chamber. All images were acquired with the Planapo 60×/1.4 oil objective lens with ×1.5 auxiliary magnification. Single-position videos in the germarium were acquired for 8 min at 25 ± 1 °C, with a 10 s temporal resolution (11-slice Z-stack, 0.5 µm per slice). For colcemid experiments, single-position videos in the germarium were acquired for 30–40 min at 25 ± 1 °C, with a 30 s temporal resolution (7-slice Z-stack, 0.7 µm per slice).

The use of α-spectrin and Par1 on fixed and live germaria respectively allowed the identification of the different cyst stages. The quantification of CID foci on fixed germaria was performed as previously described[23]. In all figures the images of fixed germaria shown are the projection of all Z-series that cover a region ranging from the first CID foci until the last CID foci seen. For live germaria, images shown are the projection of all Z-series of a single (t) projection.

Three-dimensional tracking of spinning-disc data was performed using Imaris software (Bitplane). The CID::RFP signal was tracked using the 'spots' function with an expected diameter of 0.3 µm. Automatically generated tracks were then edited manually to eliminate inappropriate connections, including connections between foci in different nuclei or between foci of different sizes or intensity when more likely assignments were apparent or multiple spots assigned to the same focus.

To remove global movements of the germarium, each nucleus containing a CID::RFP focus was assigned to the nearest fusome foci. Then, the position of the reference fusome was subtracted from each CID::RFP focus for each time point of the tracking to get the relative tracks. These relative tracks were then compiled using a custom MATLAB (MathWorks) routine that computes the minimum volume of the ellipsoid that encloses all of the three-dimensional points of the trajectory.

Analysis of centromere trajectories. Positions of individual centromeres were tracked every 10 s during 8 min to quantify the volume covered by each centromere. This raw volume was then corrected both for overall movements of the tissue and for variations in total nuclear volume. First, we subtracted the motion of the germarium using the position of the fusome as a reference within each cyst (Fig. 1g). Second, to take into account the significant decrease of the nuclear volume from GSCs to 16-cell cysts (Supplementary Fig. 1A), we computed the relative volume, which is the raw volume divided by the mean value of the nuclear volume at each stage. Finally, we normalized durations of each track by calculating the relative covered volume per second (Fig. 1h).

Analysis of correlations between tracks was done using Matlab (Mathworks, http://www.mathworks.com; Supplementary Fig. 1B). To make the analysis statistically significant, we considered only pairs of tracks $(\mathbf{r}_1, \mathbf{r}_2)$ within the same nuclei having at least 15 common time points. For all pairs, we first computed the correlation coefficient

$$R(\mathbf{r}_1, \mathbf{r}_2) = \frac{\langle (\mathbf{r}_1 - \langle \mathbf{r}_1 \rangle)(\mathbf{r}_2 - \langle \mathbf{r}_2 \rangle) \rangle}{\sqrt{\langle (\mathbf{r}_1 - \langle \mathbf{r}_1 \rangle)^2 \rangle} \sqrt{\langle (\mathbf{r}_2 - \langle \mathbf{r}_2 \rangle)^2 \rangle}}$$

R is equal to +1 when $\mathbf{r}_1$ and $\mathbf{r}_2$ are perfectly correlated, 0 when they are not and −1 when they are perfectly anti-correlated. One needs to distinguish between situations where the two tracks are actually correlated (R close to 1) and situations where they are not, while centroids move in an identical fashion (one compelling example would be two diametrically opposed centroids moving in the same direction along a circle: the two tracks are similar but R is not close to 1). For the two stages synaptonemal complex and 8-cell cyst, the numbers of pairs of tracks exhibiting strong correlation ($R \geq 0.95$) were identical (4.9% of the total amount of long-enough pairs of tracks for 8-cell cyst stage; and 5.8% for synaptonemal complex stage). To account for similarity for the remaining pairs of tracks that are not correlated, we built a coefficient g based on the distance $D = \sqrt{\mathbf{r}^2} = \sqrt{(\mathbf{r}_1 - \mathbf{r}_2)^2}$ between the two tracks: $g = 1 - \langle (\mathbf{r} \cdot \mathbf{v})^2 / \|\mathbf{r}\|^2 \|\mathbf{v}\|^2 \rangle$, where $\mathbf{v} = \mathbf{v}_1 - \mathbf{v}_2$ (with $\mathbf{v}_{1,2}$ being the difference vector of $\mathbf{r}_{1,2}$), $\| \ \|$ is the norm of the vector, and $\langle \ \rangle$ denotes the mean. g gives a value between 0 and +1 inclusive because $g = 1 - \langle \cos^2(\mathbf{r}, \mathbf{v}) \rangle$. If D is constant: $g = 1$ and the two tracks are tied (like two points belonging to a rigid body) whereas $g \sim 0.5$ stands for a random D. According to simulations, we can consider that the two tracks are moving in a homogeneous/related way when >0.75.

Reproducibility of experiments. Images in Figs 1–8 and in Supplementary Figs 2, 4 and 8 are representative images of at least 3 independent experiments.

69. Jauffred, B. *et al.* Regulation of centrosome movements by numb and the collapsin response mediator protein during *Drosophila* sensory progenitor asymmetric division. *Development* **140,** 2657–2668 (2013).
70. Gepner, J. *et al.* Cytoplasmic dynein function is essential in *Drosophila melanogaster*. *Genetics* **142,** 865–878 (1996).

DOI: 10.1038/ncb3249

nature cell biology

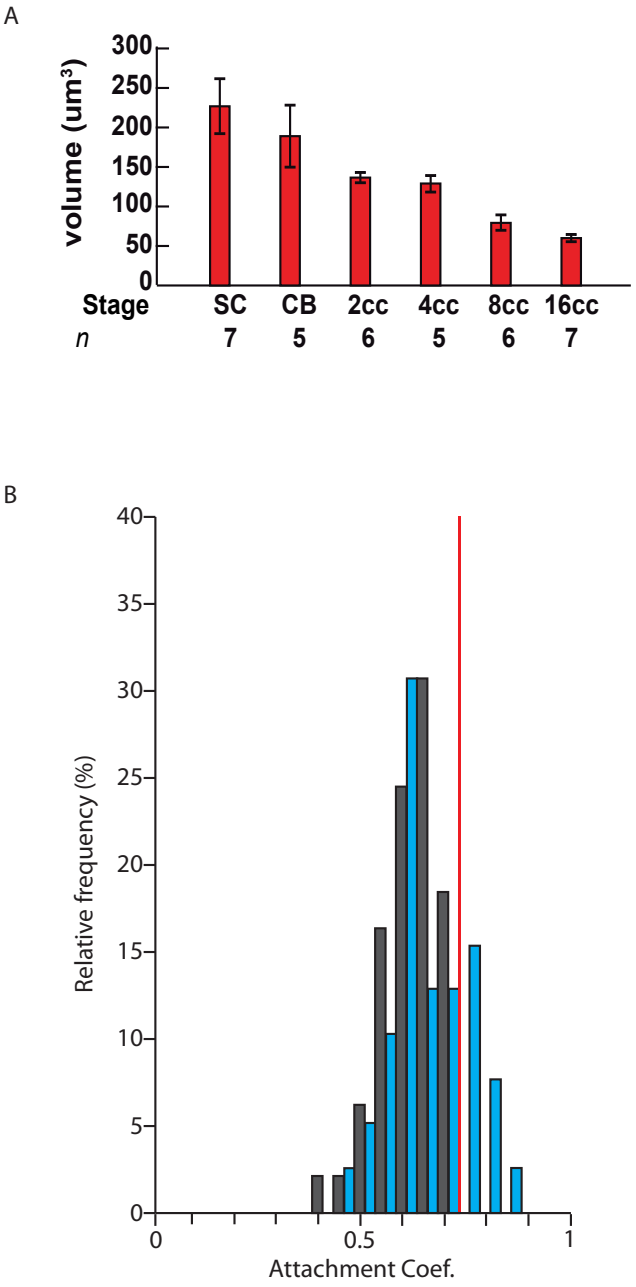

Supplementary Figure 1 (A) Mean nuclear volume for each cell stage in region 1 in Nup::GFP/+; CID::RFP/+ living germarium. For each nucleus, its longest diameter (D) and its smallest diameter (d) were determined by measuring the distance between two diametrically opposed Nup::GFP signals on projected images along the x-y axis. The height of the nucleus (h) was determined on z-series that range from the first Nup foci until the last Nup foci seen. The volume (μm^3) was calculated using the formula: V= 4 x D x d x h x π/3. The number of analyzed nuclei (n value) is indicated under each stage. Centre and error bars are mean+/- SD. **(B)** The coordinated motion between centromeres doublets at stem cell and 8cc stages. Distances between centromeres were measured in 3D time-lapse images (SC, n=41; 8cc, n=52). On the basis of the following criteria, centromere doublets were classified according to their attachment coefficient. Only doublets displaying 15 common time points and with a correlation coefficient <0,95 were taken into account for calculation of the attachment coefficient. 25% of centromere doublets display an attachment coefficient superior to 0.75 (red line) at 8cc stage (blue bars), whereas none of centromere doublets reach this value at stem cell stage (grey bars). GSC : n=49 pairs of tracks having more than 15 common time-points and correlation coefficient smaller than 0.75. 8cc : n= 39 pairs of tracks having more than 15 common time-points and correlation coefficient smaller than 0.95).

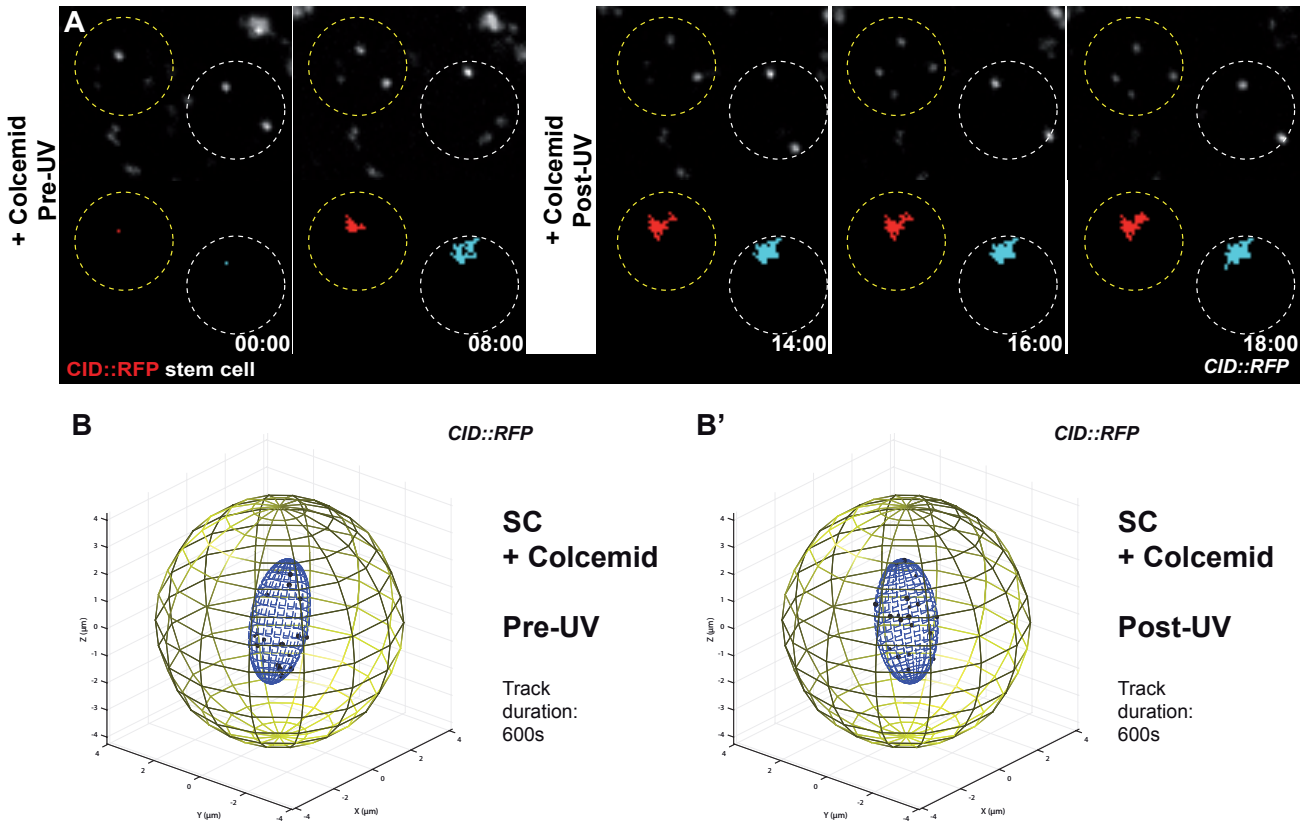

Supplementary Figure 2 (A) Inactivation by UV of the microtubule inhibitor colcemid does not affect CID foci dynamics in stem cells. Selected projections of Z-sections of single stem cells are shown. In the first two projections colcemid is active, microtubules are depolymerized and centromeric foci movement is very limited. In the last three projections colcemid was inactivated with a 5sec UV pulse and centromeric movement is not altered. For each time point, the cumulative tracking is represented in the bottom half picture. The yellow and white dotted circles indicate the nuclear surface of two nuclei in each image. (B, B') 3D representations indicating the covered volume of the selected representative track corresponding to the yellow nucleus for all time points, the ellipsoid is arbitrarily centered into a sphere representing the nuclear volume of the stem cell nucleus before the UV pulse (B) and the same 8cc after UV pulse (B').

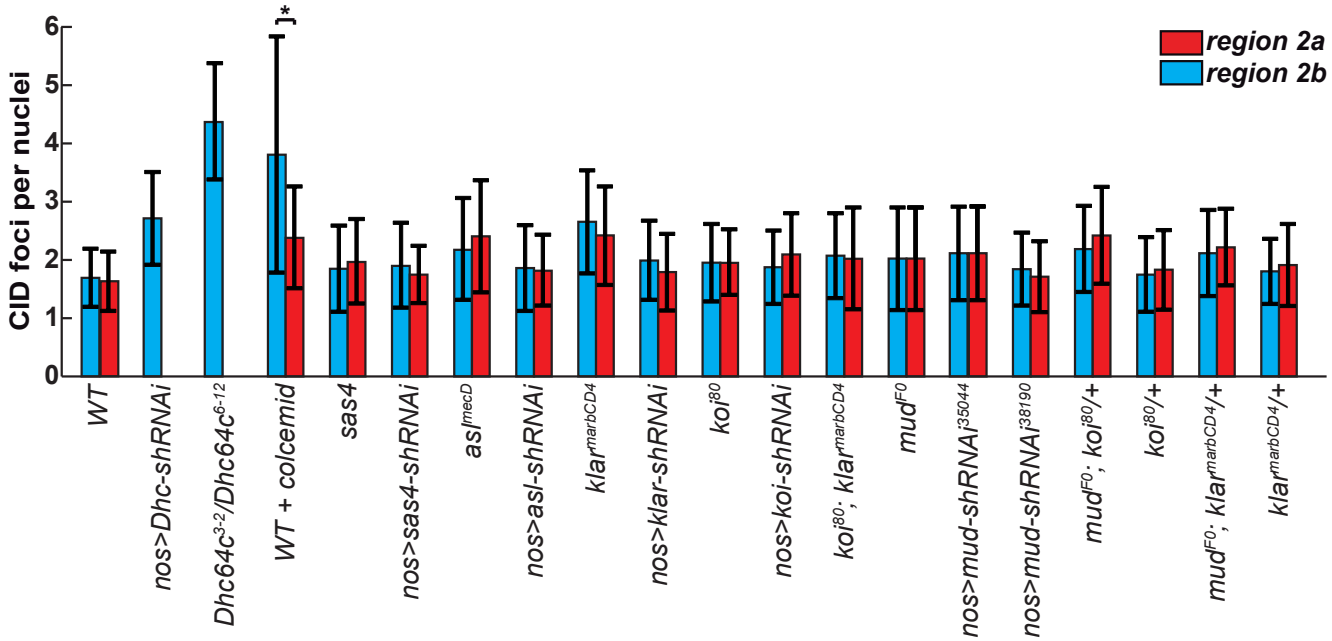

Supplementary Figure 3 Developmental changes in the number of CID foci in region 2a and 2b in fixed germarium. For each genotype, the mean number of CID foci in region 2a (blue bars) and in region 2b (red bars) is indicated.* $p<0.05$ (data collected across 3 independent experiments for each genotype; centre and error bars are mean +/- S.D). wt region 2a n=89 nuclei from 13 germarium; wt region 2b n=55 from 21 germarium; *nos>Dhc-shRNAi* region 2a n=75 nuclei from 5 germarium; *Dhc64c*$^{3-2}$*/Dhc64c*$^{6-12}$ region 2a n=224 nuclei from 6 germarium; wt + colcemid region 2a n=49 nuclei from 13 germarium; wt + colcemid in region 2b n=24 nuclei from 13 germarium; *Sas4*^{s2214} region 2a n=68 from 23 germarium; *Sas4*^{s2214} region 2b n=23 from 14 germarium; *Asl*^{MecD} region 2a n=52 nuclei from 12 germarium; *Asl*^{MecD} region 2b n=21 from 12 germarium; Sas4-RNAi region 2a n=78 from 12 germarium; Sas4-RNai region 2b n=22 from 11 germarium; asl-RNAi region 2a n=96 from 12 germarium; asl-RNAi region 2b n=22 from 12 germarium; *klar*^{marbCD4} region 2a n=102 nuclei from 13 germarium; *klar*^{marbCD4} region 2b n=45 from 30 germarium; *koi*^{80} region 2a n=71 nuclei from 13 germarium; *koi*^{80} region 2b n=47 from 29 germarium; *klar*^{marbCD4}*;koi*^{80} region 2a n=199 nuclei from 21 germarium; *klar*^{marbCD4}*;koi*^{80} region 2b n=46 nuclei from 28 germarium; klar-RNAi region 2a n=70 nuclei from 7 gerrmaria; klar-RNAi region 2b n=21 nuclei from 11 germarium; koi-RNAi region 2a n=79 nuclei from 10 germarium; koi-RNAi region 2b n=29 from 16 germarium; *mud*^{fO1205} region 2a n=131 nuclei from 15 germarium; *mud*^{fO1205} region 2b n=45 nuclei from 28 germarium; mud-RNAi (BI:35044) region 2a n=62 nuclei from 6 germarium; mud-RNAi (BI:35044) region 2b n=17 nuclei from 12 germarium; mud-RNAi (BI:38190) region 2a n=51 nuclei from 6 germarium; mud-RNAi (BI:38190) region 2b n=13 nuclei from 9 germarium; *klar*^{mbCD4}/+ region 2a n= 81 nuclei from 18 germarium; *klar*^{mbCD4}/+ region 2b n= 34 nuclei from 22 germarium; *koi*^{80}/+ region 2a n= 87 nuclei from 18 germarium; *koi*^{80}/+ region 2b n= 36 nuclei from 19 germarium; *mud*^{fO1205}*;klar*^{mbCD4}/+ region 2a n=257 nuclei from 40 germarium; *mud*^{fO1205}*;klar*^{mbCD4}/+ region 2b n=59 nuclei from 38 germarium; *mud*^{fO1205}*;koi*^{80}/+ region 2a n=86 nuclei from 19 germarium; *mud*^{fO1205}*;koi*^{80}/+ region 2b n=41 nuclei from 26 germarium.

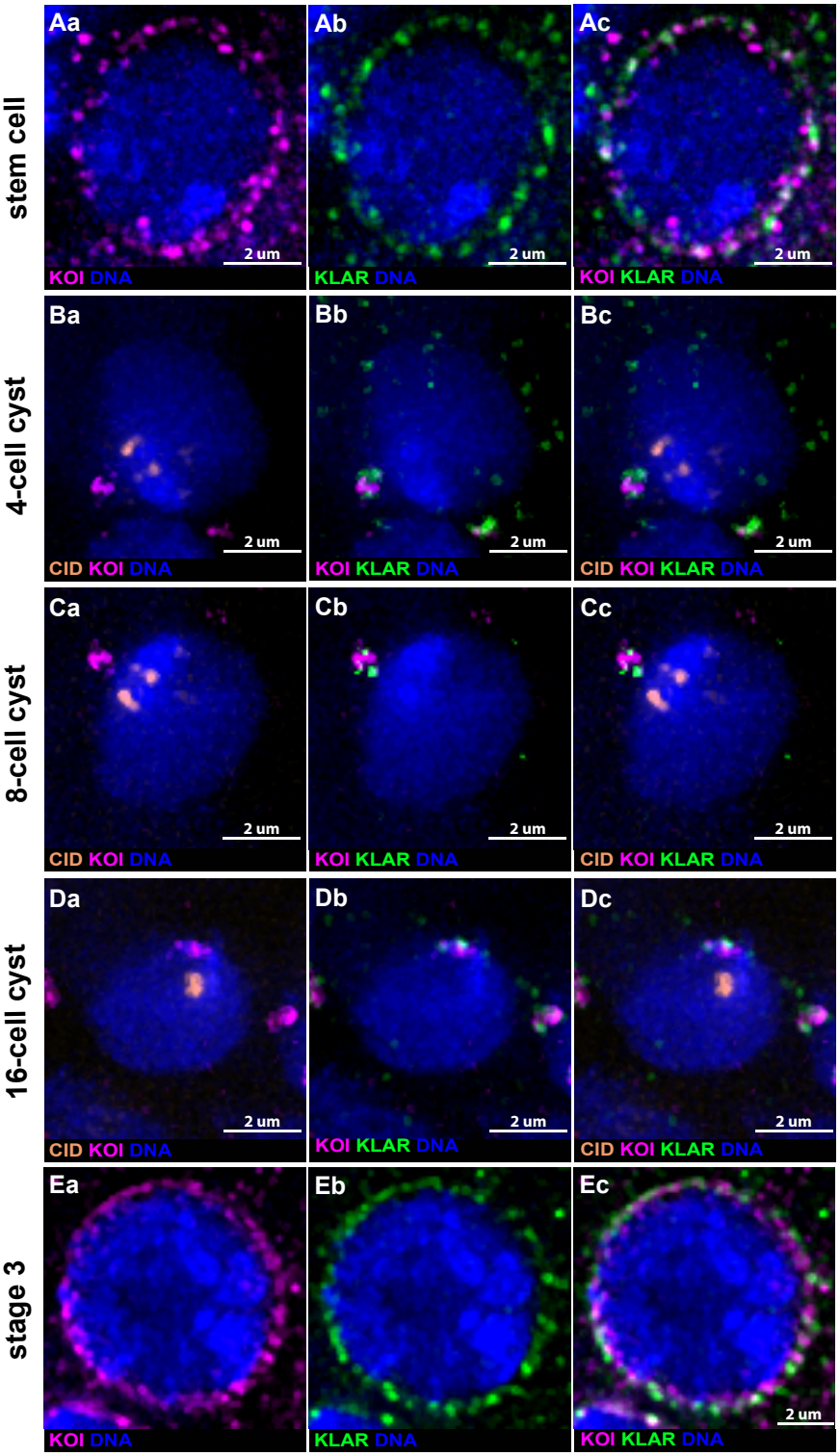

Supplementary Figure 4 Projections of Z-sections obtained by DV microscopy of a wild-type stem cell nucleus (Aa-Ac), a 4-cell cyst nucleus (Ba-Bc), an 8-cell cyst nucleus (Ca-Cc), a 16-cell cyst nucleus (Da-Dc) and a stage 3 ovocyte nucleus (Ea-Ec) stained for centromere (CID, orange), Klarsicht (Klar, green), Klaroid (Koi, magenta) and DNA (DAPI, blue). Koi and klar display a perinuclear localization in SCs and stage3 ovocytes (A, E). In some 4-cell cysts and 16-cell cysts koi and klar localize as dots at the nuclear membrane (B,D). In 8-cell cysts koi and klar localize as dots at the nuclear membrane.

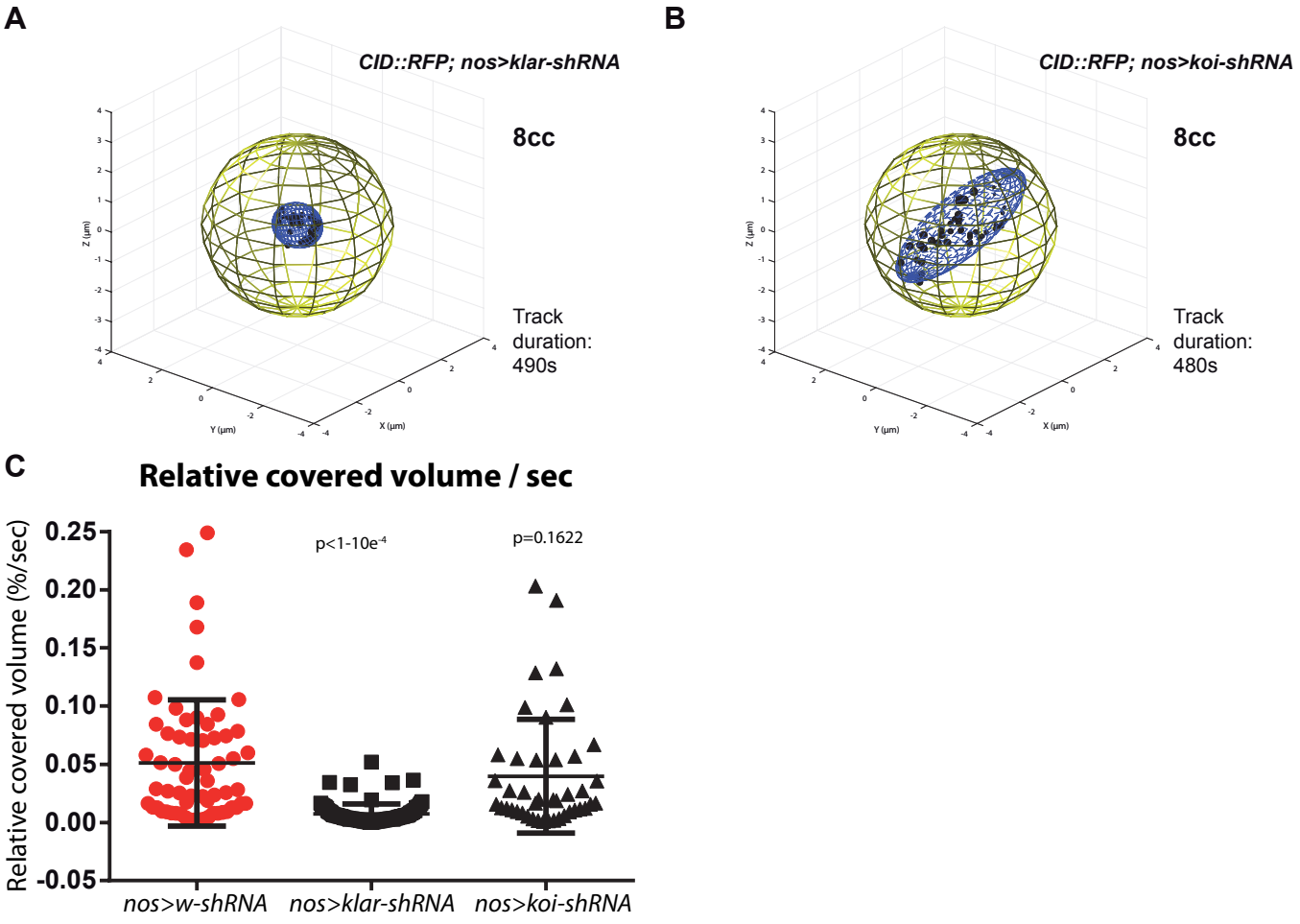

Supplementary Figure 5 (A,B) 3D representations indicating the relative covered volume of one selected representative track for all time points of a *CID::RFP;nos/klar-shRNA* (A), and a *CID::RFP, nos/koi-shRNA* (B) 8cc selected nucleus. The ellipsoid is arbitrarily centered into a sphere representing the nuclear volume (gold sphere). (C) Distributions of the relative covered volume per second· for centromeric foci in *CID::RFP;w-shRNA*, *CID::RFP;nos/klar-shRNA*, and *CID::RFP, nos/koi-shRNA* 8cc nuclei (mean+/-S.D . Mann-Whitney U-test comparing *CID::RFP;w-shRNA with CID::RFP;nos/klar-shRNA:* $p \leq 1x10^{-4}$ and with *CID::RFP, nos/koi-shRNA:* p=0.1622). nos>w-shRNA=44 centromeric foci/4 experiments; nos>klar-shRNA=94 centromeric foci/6 experiments; nos>koi-shRNA=43 centromeric foci/4 experiments.

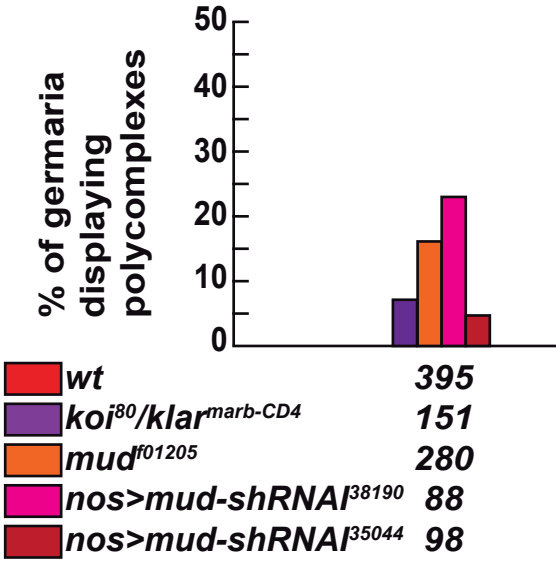

Supplementary Figure 6 Changes in the percentages of germarium displaying Polycomplexes in wild-type, *koi*^{80}; *klar*$^{marb\text{-}CD4}$, *mud*^{f01205}, *nos>mud-shRNA*^{38190} and *nos>mud-shRNA*^{35044}. The number of analyzed germarium is indicated under each stage.

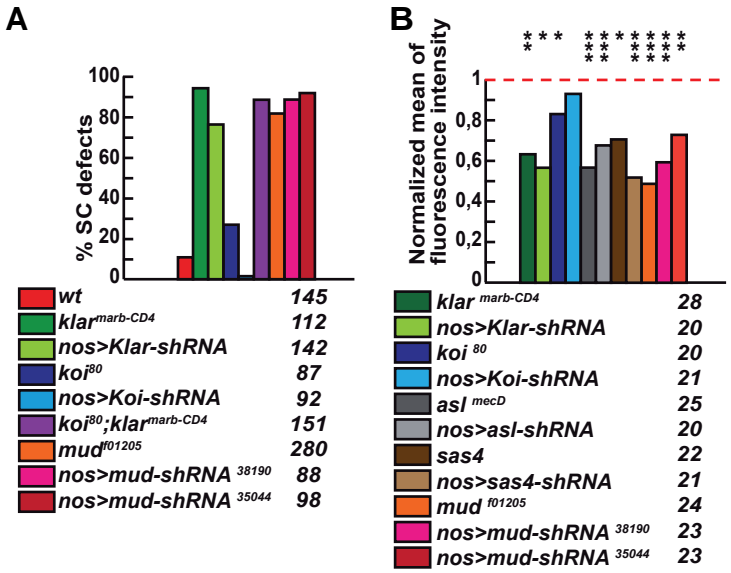

Supplementary Figure 7 (A) Changes in the percentage of germarium displaying SC defects in wild-type, *klar*$^{marb-CD4}$, *koi*^{80}, *koi*^{80}; *klar*$^{marb-CD4}$ and *mud*^{f01205}and their respective sh-RNAs (in all cases except *koi*^{80} and *koi-shRNA* khi^2<0.0005). The number of analyzed germarium is indicated for each stage. wt n=145 germarium collected across 3 independent preparations; *mud*^{f01205} n=280 germarium;3 independent preparations; mud-RNai (BI:38190) n=88;3 independent preparations; mud-RNAi (BI:35044) n=98;3 independent preparations. (B) SC fluorescence intensity was quantified in all mutant and sh-RNA conditions. Each one was normalized to the intensity of wt controls (dotted red line equal to 1) introduced in the mutant or sh-RNA preparations (3 independent experiments, error bars are mean+/-SD, two-tailed Student's t-tests * $p \leq 5x10^{-2}$, ** $p \leq 5x10^{-5}$, *** $p \leq 5x10^{-8}$) wt n=22 measurements from 22 germarium; mudf0 n=24 measurements from 24 germarium; mud-RNAi (BI:38190) n=23 measurements from 23 germarium; mud-RNAi (BI:35044) n=23 measurements from 23 germarium.

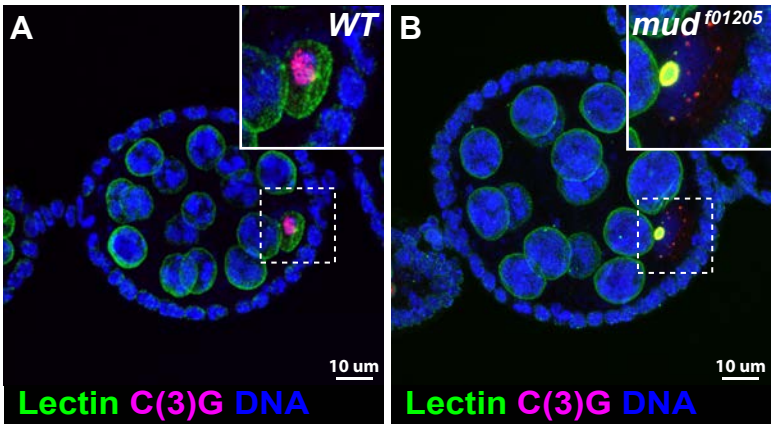

Supplementary Figure 8 Projections of Z-sections obtained by confocal microscopy of fixed wild type (A) and *mud*^{f01205} (B) stage 3 egg chambers stained for C(3)G in red, the nuclear membrane (lectin, green), and DNA. When PCs are observed in *mud*^{f01205} the DNA in the corresponding oocyte is diffuse and lectin staining is absent.

Genotype	centromere pairing in 8-cell cysts			centromere clustering in region 2a			% of germaria with synapsis defects			SC fluorescence intensity normalised to wild type		
	mean±st dev	*n*	*P*	mean±st dev	*n*	*P*	%	*n*	*P*	Normalized reduction (%)	n (shRNA/Control)	*P*
nos>klar-shRNA	4.6±1.1	86	<0.00005	2.3±0.8	70	<0.005	76.6	142	<0.00005	44	20 /21	<0.0005
nos>kol-shRNA	4.4±1.3	85	<0.005	2.2±0.7	79	<0.05	1.1	92	>0.05	8	21/21	>0.05

Genotype 1	Genotype 1 meanzst dev, n	Genotype 2	Genotype 2 meanzst dev, n	Genotype 3	Genotype 3 meanzst dev, n	Test performed	P value found	Posthoc analysis if ANOVA with P
wt	3.8±0.8, 63	*wt + colcemid*	4.7±1.5, 46			Student test	1.60E-04	
wt	3.8±0.8, 63	*nos>Dhc-shRNA*	6.0±1.7, 34			Student test	6.30E-13	
wt	3.8±0.8, 63	*sas4*$^{\Delta 2214}$ *clones*	4.7±1.6, 91			Student test	1.70E-04	
wt	3.8±0.8, 63	*nos>sas4-shRNA*	4.2±1.2, 77			Student test	6.14E-02	
wt	3.8±0.8, 63	*asl*^{mis2}	4.8±1.2, 77			Student test	7.30E-08	
wt	3.8±0.8, 63	*nos>asl-shRNA*	4.1±1.7, 76			Student test	2.10E-01	
wt	3.8±0.8, 63	*koi*^{80}	4.9±1.3, 63			Student test	1.90E-07	
wt	3.8±0.8, 63	*klar*$^{\Delta wdc2d}$	5.1±1.3, 78			Student test	1.70E-09	
wt	3.8±0.8, 63	*klar*$^{\Delta wdc2d}$, *koi*^{80}	5.6±1.4, 61			Student test	9.00E-15	
wt	3.8±0.8, 63	*nos>koi-shRNA*	4.4±1.3, 85			Student test	2.00E-03	
wt	3.8±0.8, 63	*nos>klar-shRNA*	4.6±1.1, 86			Student test	2.80E-05	
wt	3.8±0.8, 63	*mud*^{E1359}	4.3±1.2, 77			Student test	1.70E-02	
wt	3.8±0.8, 63	*nos>mud-shRNA*^{BL180}	4.2±1.2, 93			Student test	1.80E-02	
wt	3.8±0.8, 63	*nos>mud-shRNA*^{BL64}	4.0±1.3, 94			Student test	3.40E-01	
wt	3.8±0.8, 63	*koi*^{80}/+	3.5±0.4, 45			Student test	5.30E-02	
wt	3.8±0.8, 63	*klar*$^{\Delta wdc2d}$/+	4.0±0.4, 74			Student test	4.40E-01	
wt	3.8±0.8, 63	*mud*^{E1359}, *klar*$^{\Delta wdc2d}$/+	5.2±1.2, 83			Student test	6.80E-13	
wt	3.8±0.8, 63	*mud*^{E1359}, *koi*^{80}/+	4.7±1.3, 94			Student test	2.30E-06	
koi^{80}/+	3.5±0.4, 45	*mud*^{E1359}	4.3±1.2, 77	*mud*^{E1359}, *koi*^{80}/+	4.7±1.3, n=94	ANOVA	3.10E-07	Student test with a Bonferonni correction. All pairwise comparisons displayed statistically significant differences (p<0.0167)
klar$^{\Delta wdc2d}$/+	4.0±0.4, 74	*mud*^{E1359}	4.3±1.2, 77	*mud*^{E1359}, *klar*$^{\Delta wdc2d}$/+	5.2±1.2, n=83	ANOVA	3.40E-10	Student test with a Bonferonni correction. Statistically significant differences were found when comparing 1/mudf0 and mudf0; klar/+ 2/klar/+ and mudf0;klar/+ (p<0.000017)

Genotype 1	Genotype 1 meanŁst dev, n	Genotype 2	Genotype 2 meanŁst dev, n	Genotype 3	Genotype 3 meanŁst dev, n	Test performed	P value found	Posthoc analysis if ANOVA with P
wt	2.0±0.6, 89	*wt + colcemid*	4.4±2.4, 49			Student test	1.90E-16	
wt	2.0±0.6, 89	*nos>Dhc-shRNA*	3.2±0.9, 76			Student test	1.00E-18	
wt	2.0±0.6, 89	*Dhc64C$^{3-2}$/Dhc64C$^{6-12}$*	5.1±1.2, 224			Student test	1.70E-73	
wt	2.0±0.6, 89	*sas4^{S2214} clones*	2.2±0.9, 67			Student test	1.10E-01	
wt	2.0±0.6, 89	*nos>sas4-shRNA*	2.2±0.9, 78			Student test	2.50E-02	
wt	2.0±0.6, 89	*asl^{mk2}*	2.6±1.0, 52			Student test	3.10E-05	
wt	2.0±0.6, 89	*nos>asl-shRNA*	2.2±0.9, 96			Student test	6.80E-02	
wt	2.0±0.6, 89	*koi^{80}*	2.3±0.8, 71			Student test	5.30E-03	
wt	2.0±0.6, 89	*klar^{mk3CD4}*	3.1±1, 102			Student test	1.50E-16	
wt	2.0±0.6, 89	*klar^{mk3CD4}, koi^{80}*	2.4±0.8, 199			Student test	1.10E-04	
wt	2.0±0.6, 89	*nos>koi-shRNA*	2.2±0.7, 79			Student test	3.90E-02	
wt	2.0±0.6, 89	*nos>klar-shRNA*	2.3±0.8, 70			Student test	1.60E-03	
wt	2.0±0.6, 89	*mud^{ff1309}*	2.4±1.0, 131			Student test	1.80E-03	
wt	2.0±0.6, 89	*nos>mud-shRNA^{28044}*	2.4±0.9, 62			Student test	1.20E-04	
wt	2.0±0.6, 89	*nos>mud-shRNA^{28190}*	2.1±0.7, 51			Student test	1.10E-01	
wt	2.0±0.6, 89	*koi^{80}/+*	2.0±0.7, 87			Student test	5.00E-01	
wt	2.0±0.6, 89	*klar^{mk3CD4}/+*	2.1±0.7, 81			Student test	1.60E-01	
wt	2.0±0.6, 89	*mud^{ff1309}, klar^{mk3CD4}/+*	2.5±0.9, n=257			Student test	7.00E-07	
wt	2.0±0.6, 89	*mud^{ff1309}, koi^{80}/+*	2.6±0.9, n=86			Student test	4.80E-07	
koi^{80}/+	2.0±0.7, 87	*mud^{ff1309}*	2.4±1.0, 131	*mud^{ff1309}, koi^{80}/+*	2.6±0.9, n=86	ANOVA	<0.005	Student test with a Bonferonni correction. Statistically significant differences were found when comparing 1/koi80/+ and mudf0 2/koi80/+ and mudf0; koi80/+ (p<0.0167)
klar^{mk3CD4}/+	2.1±0.7, 81	*mud^{ff1309}*	2.4±1.0, 131	*mud^{ff1309}, klar^{mk3CD4}/+*	2.5±0.9, n=295	ANOVA	<0.01	Student test with a Bonferonni correction. Statistically significant differences were found when comparing 1/klar/+ and mudf0; klar/+ (p<0.0017)

Supplementary Table Legends

Supplementary Table 1 Defects induced by klarsicht and klaroid shRNAs on centromere pairing and synapsis. The Student t-test was used to measure each statistical significance, except for % of germaria with synapsis defects, where a khi2 test was performed.

Supplementary Table 2 Defects induced by mutations and shRNAs on centromere pairing (8cc). Pairwise tests were made using Student t-tests. Comparison between multiple genotypes were made using ANOVA followed by pairwise Student t-test with a Bonferroni correction.

Supplementary Table 3 Defects induced by mutations and shRNAs on clustering (region 2a). Pairwise tests were made using Student t-tests. Comparison between multiple genotypes were made using ANOVA followed by pairwise Student t-test with a Bonferroni correction.

Supplementary Video Legends

Supplementary Video 1 Dynamics of centromere clusters in region 1. Time lapse microscopy (spinning disc) of a germarium expressing the centromere marker CID::RFP (red) and the fusome marker Par1::GFP (green). Three germinal stem cells (GSC) are identified by their position close to the niche and their spectrosome. The upper cystoblast (CB) is identified by its round fusome, and the 2-cell cyst (2cc), whose cells are linked by a snowman-shaped fusome. Four nuclei of an 8-cell cyst (8cc), whose cells are linked by a branched-shaped fusome, demonstrating that they are from the same cyst. Arrow points towards rotating centromeres cluster in an 8cc. Frames were taken every 10 seconds. The video is shown at 3 frames/s (MPEG4).

Supplementary Video 2 Dynamics of Nuclear membrane in a rotating 8cc nucleus. Time lapse microscopy (spinning disc) of a germarium expressing the centromere marker CID::RFP (red), the nuclear membrane marker Nup::GFP (green). Frames were taken every 10 seconds. The movie is shown at 7 frames/s (MPEG4).

Supplementary Video 3 Dynamics of chromatin in living 8-cell cysts. Time lapse microscopy (spinning disc) of a germarium expressing the centromere marker CID::RFP (red) and the histone marker H2::dendra (green, red). Photo-conversion occurred just after the first z-acquisition, by applying 10 pulses of 0.054 sec of 405 nm laser on the ROI. Frames were taken every 10 seconds. The movie is shown at 7 frames/s (MPEG4).

Supplementary Video 4 Centrosome and microtubules dynamics in living wild-type 8-cell cysts. Time lapse microscopy (spinning disc) of a germarium expressing the centromere marker CID::RFP (red), the centrosome marker asl::YFP and the microtubule associated protein Jupiter::GFP (green). The movie is shown at 7 frames/s (MPEG4).

Supplementary Video 5 Microtubule dynamics in UV pulse and Colcemid treated living 8-cell cysts. Time lapse microscopy (spinning disc) of a colcemid-treated germarium expressing the centromere marker CID::RFP (red) and the microtubule-associated protein jupiter::GFP (green). A 5 sec UV pulse was performed at t=10:00, illustrated by a light blue flash. Frames were taken every 30 seconds. The movie is shown at 7 frames/s (MPEG4).

Supplementary Video 6 Microtubule, centrosomes and centromeres dynamics in UV pulse and Colcemid treated living 8-cell cysts. Time lapse microscopy (spinning disc) of a colcemid-treated germarium expressing the centromere marker CID::RFP (red) , the microtubule-associated protein jupiter::GFP (green) and the centrosome associated protein asterless::YFP (green). A 5 sec UV pulse was performed at t=2:00, illustrated by a light blue flash. Frames were taken every 30 seconds. The movie is shown at 7 frames/s (MPEG4). Filled arrowheads point to the fusome, empty arrowheads point to centrosome, and arrows point to the cell membrane (MPEG4).

Supplementary Video 7 Centrosomes rotate in the same direction and with the same speed as centromeres in living 8-cell cysts. Time lapse microscopy (spinning disc) of germarium expressing the centromere marker CID::RFP (red) and the centrosome marker asl::YFP (green). Frames were taken every 10 seconds. The movie is shown at 7 frames/s (MPEG4).

Supplementary Video 8 Colcemid treatment leads to inhibition of CID foci dynamics in living 8-cell cysts. Time lapse microscopy (spinning disc) of a colcemid-treated germarium expressing the centromere marker CID::RFP. Frames were taken every 10 seconds. The movie is shown at 7 frames/s (MPEG4).

Supplementary Video 9 Centromere dynamics in UV pulse and Colcemid treated in living 8-cell cysts. Upper panel: Time lapse microscopy (spinning disc) of a colcemid-treated germarium expressing the centromere marker CID::RFP . A 5 sec UV pulse was performed at t=10:00, illustrated by a light blue flash. Bottom panel: Tracking of two CID::RFP clusters before and after the UV pulse. The circles illustrates the maximal area covered before (yellow) and after (pink) UV pulse. Frames were taken every 30 seconds. The movie is shown at 7 frames/s (MPEG4).

Supplementary Video 10 Centrosome dynamics in UV pulse and Colcemid treated in living 8-cell cysts. Time lapse microscopy (spinning disc) of a living colcemid-treated germarium expressing the centromere marker CID::RFP (red), the centrosome marker asl::YFP and the microtubule associated protein Jupiter::GFP (green). A 5 sec UV pulse was performed at t=2:00, illustrated by a light blue flash. Frames were taken every 30 seconds. The movie is shown at 7 frames/s (MPEG4).

Supplementary Video 11 Centromere dynamics in UV pulse and Colcemid treated in living stem cell.
Upper panel: Time lapse microscopy (spinning disc) of a colcemid-treated germarium expressing the centromere marker CID::RFP . A 5 sec UV pulse was performed at t=10:00, illustrated by a light blue flash. Bottom panel: Tracking of two CID::RFP clusters before and after the UV pulse. The circles illustrates the maximal area covered before (yellow) and after (pink) UV pulse. Frames were taken every 30 seconds. The movie is shown at 7 frames/s (MPEG4).

Supplementary Video 12 *white* loss of function by RNAi does not affect CID foci dynamics in living 8-cell cysts. Time lapse microscopy (spinning disc) of a *w-shRNA* ^{35573} germarium expressing the centromere marker CID::RFP. Frames were taken every 10 seconds. The movie is shown at7 frames/s (MPEG4).

Supplementary Video 13 *sas-4* loss of function by shRNA leads to inhibition of CID foci dynamics in living 8-cell cysts.Time lapse microscopy (spinning disc) of a *sas-4-shRNA*^{35049} germarium expressing the centromere marker CID::RFP. Frames were taken every 10 seconds. The movie is shown at 7 frames/s (MPEG4).

Supplementary Video 14 *asl* loss of function by shRNA leads to inhibition of CID foci dynamics in living 8-cell cysts. Time lapse microscopy (spinning disc) of a *asl-shRNA*^{35039} germarium expressing the centromere marker CID::RFP. Frames were taken every 10 seconds. The movie is shown at 7 frames/s (MPEG4).

Supplementary Video 15 *Dynein* loss of function by shRNA leads to inhibition of CID foci dynamics in living 8-cell cysts. Time lapse microscopy (spinning disc) of a *Dhc64C-shRNA*^{36583} germarium expressing the centromere marker CID::RFP. Frames were taken every 10 seconds. The movie is shown at 7 frames/s (MPEG4).

Supplementary Video 16 *Dynein* loss of function in *Dhc64C*$^{3-2}$ */Dhc64C*$^{6-12}$ mutant leads to inhibition of CID foci dynamics in living 8-cell cysts. Time lapse microscopy (spinning disc) of a *Dhc64C*$^{3-2}$ */Dhc64C*$^{6-12}$ mutant germarium expressing the centromere marker CID::RFP. Frames were taken every 10 seconds. The movie is shown at 7 frames/s (MPEG4).

Supplementary Video 17: Centrosome and microtubule dynamics in living *Dynein* mutant 8-cell cysts. Time lapse microscopy (spinning disc) of a *Dhc64c*$^{6\text{-}12}$/ *Dhc64c*$^{3\text{-}2}$ mutant germarium expressing the centromere marker CID::RFP (red), the centrosome marker asl::YFP and the microtubule associated protein Jupiter::GFP (green). The movie is shown at 7 frames/s (MPEG4).

Supplementary Video 18 CID-RFP and KASH-GFP remain in close proximity in living 8-cell cysts. Time lapse microscopy (spinning disc) of germarium expressing the centromere marker CID::RFP (red) and the KASH domain KASH::GFP (green). Frames were taken every 20 seconds. The movie is shown at 7 frames/s (MPEG4).

Supplementary Video 19 *klarsicht* loss of function leads to inhibition of CID foci dynamics in living 8-cell cysts. Time lapse microscopy (spinning disc) of a *klar*^{marbCD4} germarium expressing the centromere marker CID::RFP. Frames were taken every 10 seconds. The movie is shown at 7 frames/s (MPEG4).

Supplementary Video 20 *klaroid* loss of function displays CID foci dynamics in living 8-cell cysts. Time lapse microscopy (spinning disc) of a *koi*^{80} germarium expressing the centromere marker CID::RFP. Frames were taken every 10 seconds. The movie is shown at 7 frames/s (MPEG4).

Supplementary Video 21 CID foci dynamics in wild type 8-cell cysts. Time lapse microscopy (spinning disc) of a germarium expressing the centromere marker CID::RFP . Frames were taken every 30 seconds. The movie is shown at 7 frames/s (MPEG4).

Supplementary Video 22 *mud* loss of function does not affect CID foci dynamics in living 8-cell cysts. Time lapse microscopy (spinning disc) of a *mud*^{f01205} mutant germarium expressing the centromere marker CID::RFP. Frames were taken every 30 seconds. The movie is shown at 7 frames/s (MPEG4).